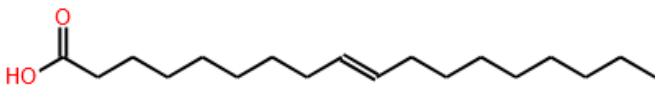
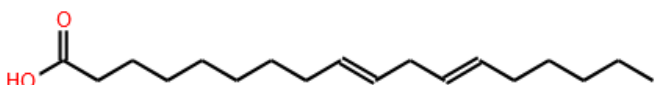


3. Biobased plasticizer production process

After selecting a potentially suitable plasticizing molecule based on the different performance criteria, the next stage of this work was to design a production process that considers the effect of the main variables during the reaction and separation stages. Although the target molecule is an epoxide of isobutyl soyate, the experimental work was performed using three additional feedstocks: oleic acid, linoleic acid, and a distillation fraction obtained from the SODD. Evaluating feedstocks with similar fatty acid composition provides a better understanding of the reaction and separation stages. The different raw materials used in the experimental work are presented in Table 3-1.

Table 3-1. Fatty acid - raw materials used in the experimental design.

| Feedstock | Chemical nature |
|---|--|
| A) Oleic acid (OA) |  |
| B) Linoleic acid (LA) |  |
| C) Soybean oil deodorizer distillate (SODD) | Mixture of saturated and unsaturated fatty acids (C16-C18) and acylglycerols. |

This chapter outlines the production of isobutyl epoxides from soybean oil and its derivatives (i.e., linoleic acid, oleic acid, and SODD). The choice of these raw materials was based on the fact that linoleic acid (C18:2) is the main fatty acid in the lipid profile of SODD, while oleic acid has an iodine value similar to that of SODD, which is the valuable agro-industrial residue of interest.

The proposed process involves two reaction steps (i.e. esterification and epoxidation), and different reaction conditions were explored to select the best processing conditions. Besides the production of epoxidized esters, this chapter also delves into the kinetics of epoxidation of isobutyl linoleate catalyzed by a homogeneous acid, and a regressed mathematical expression of the process was obtained. As the processing of each raw material is different, a simplified scheme is presented in Figure 3-1. There are minor differences in the processing of the various raw materials due to their composition, but the unit operations remain largely the same.

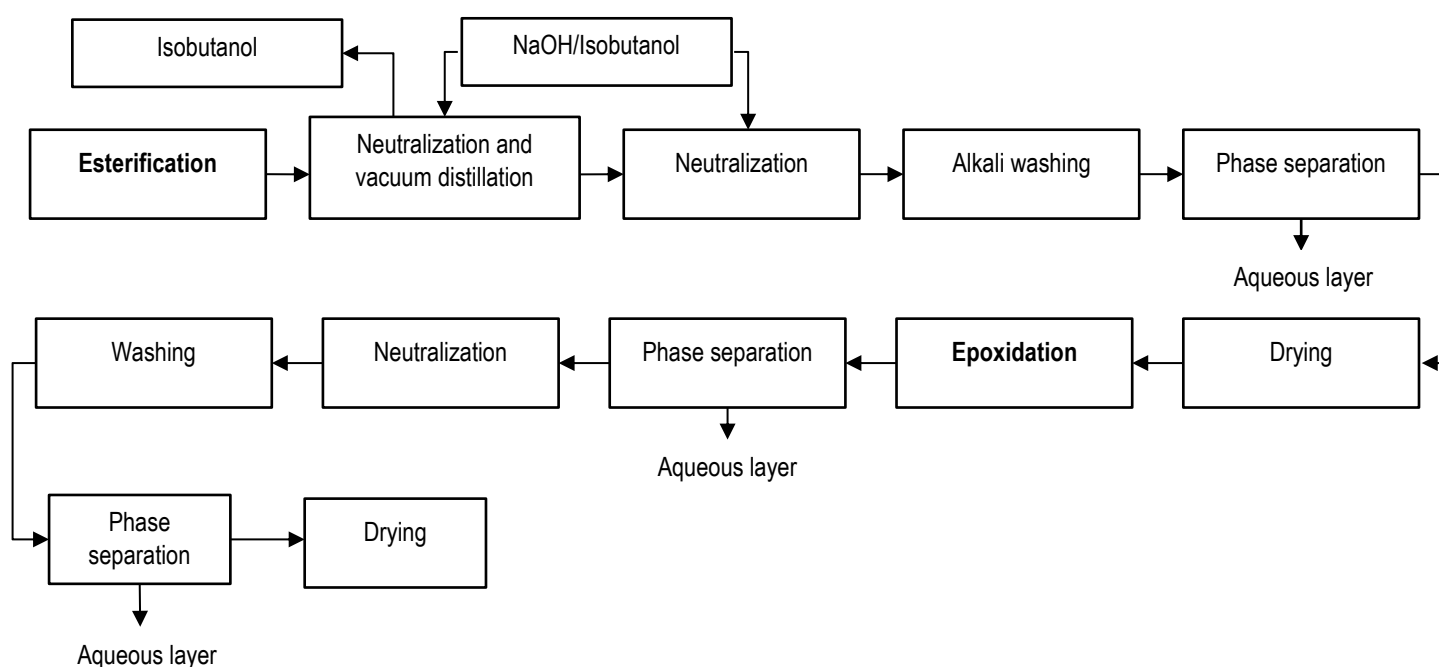


Figure 3-1. Simplified block diagram of the epoxidized isobutyl esters production process

3.1 Methodology

- Reagents

Food-grade linoleic acid ($\geq 95\%$ wt., Sigma Aldrich), technical-grade oleic acid ($>50\%$ wt. Quimiescencias), and soybean oil deodorizer distillate provided by Team Foods were used as the fatty acid reactant during esterification reactions, along with isobutanol ($> 99\%$ GC, Merck). Sulfuric acid (96% wt., Merck) was used as a catalyst. Glacial acetic acid (100% wt., J.T Baker), amberlite IRC 120 H (Merck), and aqueous hydrogen peroxide (50% wt., Chemi) were used during epoxidations. Absolute ethanol USP (PanReac), NaOH (99% wt.,

Supelco), and Toluene (99.98% wt., J.T. Baker), chloroform (HPLC grade, J.T. Baker), Wijs reagent (0.2N, PanReac), diethyl ether (99% wt., Loba Chemie PVT LTD), acetone (USP, Panreac), sodium thiosulphate pentahydrate (Supelco), hydrochloric acid (0.5M Panreac), and 2-Propanol USP (PanReac) were used during acid value, iodine index, saponification value, unsaponifiable matter, peroxide value and oxirane oxygen determination.

- **Methods**

The fatty acids (OA, LA, SODD) were characterized through acid value, iodine value, and saponification value following the official method ISO 660, ISO 3961, and ISO 3657 respectively [134],[135],[136]. The peroxide value of the SODD was measured following the official method ISO 3960 [137], while the unsaponifiable matter was measured according to ISO 3596 [138]. Each analysis was performed in triplicate. Fatty acid profiles were obtained for all raw materials by gas chromatography using a reported standard method for FAMES quantification (AOCS Ce 1-e91). FAMES were prepared from the corresponding fatty acid samples following AOCS Ce 2-66 standard method. A 7890A Agilent GC with a flame ionization detection (GC-FID) was employed using hydrogen as carrier gas.

The acid number and moisture content were analyzed using a Karl Fisher volumetric titrator (Mettler Toledo). Each analysis was performed in duplicate.

Differential Scanning Calorimetry analysis (DSC) was performed using a Mettler Toledo calorimeter 500/2722. Thermal properties of the samples, including crystallization (T_c) and melting temperatures (T_m), were evaluated by performing the following thermal cycle at a constant rate of 5 K/min: heating from 25 to 60 °C, isotherm holding for 10 min, cooling from 60 to -60°C, isotherm holding for 10 min, and heating from -60 to 60°C under a constant flow rate of N₂ of 50 ml/min.

Thermogravimetric analysis (TGA) was performed on a TGA SF/1100/268. Samples were heated from 30 to 700°C at a constant heating rate of 10°K/min. Nitrogen was used as purge gas at a flow of 60ml/min and the balance purge flow of air.

Rheological properties were measured at 20 and 40°C. Density was measured in a Densito 30PX Mettler Toledo equipment and viscosity was measured using a viscosimeter Koehler instrument equipped with a capillary viscosimeter and thermocouple.

The cloud point of the fatty acids was measured according to the standard ASTM D2500 [139]. Samples of 25 ml were cooled in a flask in a thermostatic bath set at -24°C.

FTIR spectra were carried out in an FT-IR Perkin Elmer Spectrum BX. The spectra were scanned in the range of 800 to 200 cm⁻¹ at a scan rate of 600 nm/min.

3.2 Esterification

3.2.1 Results

- Characterization of Fatty acids

The fatty acid profiles of the oleic acid (OA), linoleic acid (LA), and SODD used in this work are reported in Table 3-2. As expected, unsaturated acids, mainly oleic and linoleic, are the major components of these raw materials. The total percentages of unsaturated acids were 93.7, 99.8 and 81.3 % respectively. Considering the total number of unsaturated acids, the concentration of oxirane oxygen (OO) in the final epoxidized fatty esters is expected to follow the order LA > OA > SODD. The lipid profile of SODD was found to be consistent with that of soybean oil [140], and this is also presented in Table 3-2. For comparison purposes, a picture of the as-received fatty acid feedstocks is presented in Figure 3-2, The SODD was dark and semi-solid while the OA was a clear liquid.

Table 3-2. Fatty acid composition

| Fatty acid | OA | LA | SODD | Soybean oil [140] |
|------------|-------|-------|-------|-------------------|
| C16:0 | 3.47 | 0.20 | 13.79 | 8-14 |
| C18:0 | 2.80 | 0.05 | 4.91 | 3-5 |
| C18:1 | 55.06 | 2.35 | 30.00 | 20-25 |
| C18:2 | 34.15 | 97.21 | 47.61 | 50-57 |
| C18:3 | 0.37 | 0.19 | 3.70 | 6-8 |
| C20:2 | 2.89 | - | - | - |
| C20:3 | 1.26 | - | - | - |
| SFA (%) | 6.27 | 0.25 | 18.70 | 11-19 |
| MUFA (%) | 55.06 | 2.35 | 30.00 | 20-25 |
| PUFA (%) | 38.67 | 97.40 | 51.31 | 56-65 |

SFAA: saturated fatty acids,
 MUFA: monounsaturated fatty acids,
 PUFA: polyunsaturated fatty acids



Figure 3-2. Pictures of the employed fatty acids during esterification experiments

a) Oleic acid b) Linoleic acid c) SODD

The main physicochemical characteristics of the fatty acids used as reactants in this study are presented in Table 3-2. As can be seen, all these raw materials have a high iodine value (> 114 mg KOH/g) which is consistent with their high content of unsaturations. These high values of unsaturations are suitable for the epoxidation processes.

Table 3-3. Physicochemical properties of fatty acid feedstocks

| Property | OA | LA | SODD |
|---|-----------------|-----------------|------------------|
| Acid value (mg KOH/g) | 194.0 \pm 0.8 | 193.7 \pm 0.3 | 89.2 \pm 0.1 |
| FFA (oleic) (%) | 97.7 \pm 0.4 | 97.5 \pm 0.2 | 44.9 \pm 0.1 |
| Iodine value (g I ₂ /100g) | 120 \pm 0.6 | 176 \pm 0.2 | 114.5 \pm 0.07 |
| Saponification value (mg KOH/g) | -- | -- | 162 \pm 1 |
| Peroxide value (meg/kg) | -- | -- | 6.2 |
| Unsaponifiable matter (%) | -- | -- | 16 |
| Neutral oil (% wt.) | -- | -- | 39 |
| Moisture (%wt.) | 0.1 \pm 0.004 | 0.21 \pm 0.01 | -- |
| Density (20°C) (kg/m ³) | 901.4 \pm 0.1 | 913.0 \pm 0.1 | 911.8 \pm 0.8 |
| Density (40°C) (kg/m ³) | 883.2 \pm 0.1 | 893.0 \pm 0.1 | 893.8 \pm 0.1 |
| Kinematic Viscosity cSt (40°C) | 18.8 \pm 0.1 | 21.3 \pm 0.1 | 26 \pm 0.24 |
| Dynamic Viscosity cP (40°C) | 16.6 \pm 0.1 | 19.1 \pm 0.1 | 23.2 \pm 0.2 |
| Calculated | | | |
| MW (g/gmol) | 282.0 | 280.5 | 277.9* |
| Iodine value Theoretical (g I ₂ /100g) | 120.2 | 178.6 | 123.1 |
| Average insaturations | 1.3 | 2.0 | 1.3 |

* Acylglycerols: 100-FFA-Unsaponifiable matter

* Average molar mass of FFA calculated based on the lipid profile

Regarding the SODD, its FFA content was around 45% wt., in addition to these FFAs, this feedstock also contains a significant amount of other components, such as monoglycerides (MG), diglycerides (DG), and triglycerides (TG). The presence of these acylglycerols is confirmed by its high saponification value (162 mg KOH/g), indicating that the SODD contains various saponifiable species. Based on the saponification value of SODD, and assuming only acylglycerides of linoleic acid, it is possible to estimate their total content in the sample, as is shown in equation (3-1).

$$SV_{SODD} = x_{FFA} * SV_{FFA} + x_{TG} * SV_{TG} + x_{DG} * SV_{DG} + x_{MG} * SV_{MG} + x_{UM} * SV_{UM} \quad (3-1)$$

$$162 = x_{FFA} * 201.9 + x_{TG} * 193.1 + x_{DG} * 183.4 + x_{MG} * 159.5 + 0.16 * SV_{UM}$$

$$x_{FFA} + x_{TG} + x_{DG} + x_{MG} + x_{UM} = 1$$

$$x_{TG} + x_{DG} + x_{MG} = 0.39$$

Here, x_{MG} , x_{DG} , x_{TG} , x_{UM} are the mass fraction of monoglycerides (MG), diglycerides (DG), triglycerides (TG), and unsaponifiable matter (UM) respectively. SV_{MG} , SV_{DG} , SV_{TG} , are the saponification value of monoglycerides (MG), diglycerides (DG), and triglycerides (TG), respectively. As observed, the total content of acylglycerides remaining in SODD is around 39% wt.

Regarding the content of unsaponifiable matter (16%), it agrees with the reported values (11-33%) [16]. This high value is derived from the content of typical secondary metabolites encountered in soybean oil such as tocopherols, lecithin, sterols, and squalene. The peroxide value (6.2 meq O₂/kg) was measured to estimate the oxidative stability of the SODD. This result indicates a low content of oxidative components such as ketones and aldehydes.

The results from the physicochemical and rheological characterization of samples are also presented in Table 3-3. Among the assessed properties, viscosity is an important parameter for a plasticizer application. According to these values, the viscosity of FFA decreases in the order: SODD>LA>OA. It is expected that the epoxides of the respective FFA would follow the same trend.

- Thermal characterization of the fatty acids

To study the thermal properties of the feedstocks (OA, LA, and SODD), the samples were analyzed using two thermal cycles, one cycle of cooling (crystallization cycle) and one of heating (melting cycle) through controlled thermal conditions. The results are displayed in Figure 3-3, Figure 3-4, and Figure 3-5, and are summarized in Table C-1, Table C-2, and Table C-3 in Annex C – Thermal properties.

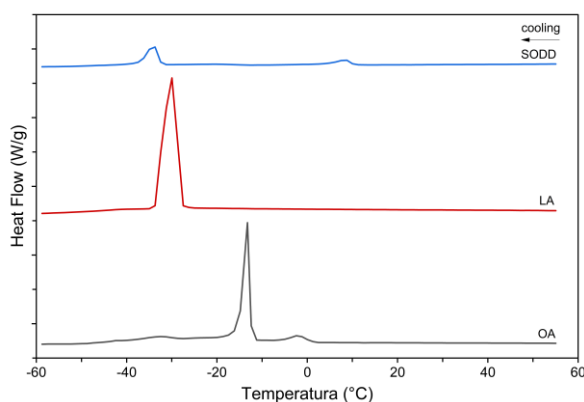


Figure 3-3. Crystallization DSC curves of FFA

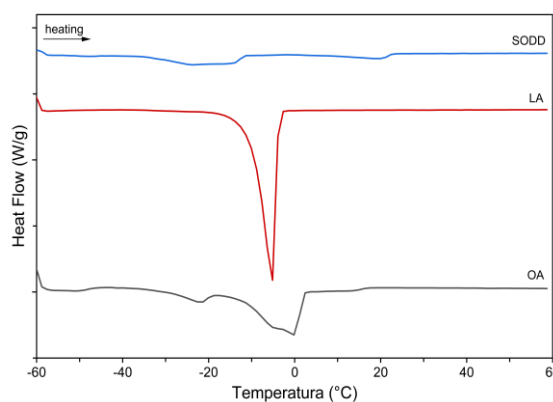


Figure 3-4. Melting DSC curves of FFA

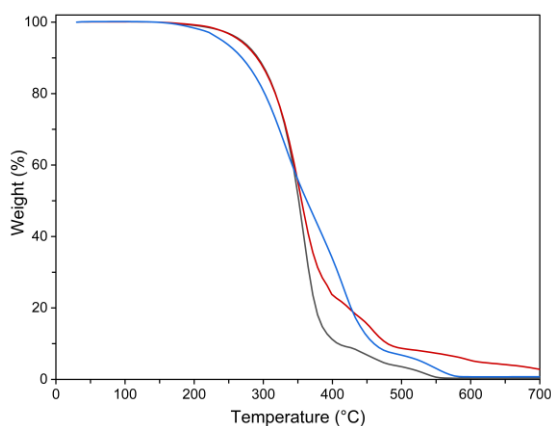


Figure 3-5. Thermal degradation of FFA.

(— OA) (—LA) (—SODD)

Melting and crystallization curves for oleic acid show two characteristic peaks, as reported in the literature [141]. In the cooling cycle (exothermic phase transition), OA exhibits two peaks at -1.7°C and -13.1°C which are associated to the crystallization of the meta-stable

α -form and the γ polymeric transformation [142]. For the melting cycle (endothermic phase transition), the major peak is found at 0°C. This point differs from the melting temperature of OA which ranges from 13.2°C to 16.3°C [130]. This significant difference was expected as a commercial brand of Oleic acid with a technical grade purity of ~50% wt. was employed in this study. The crystallization temperature (T_c) and cloud point of LA were -30°C and -22°C, respectively. According to these curves, low freezing temperatures were achieved due to a high content of unsaturated fatty acids. These low freezing temperature values indicate good low-temperature performance, which is valuable for lubricant or plasticizing applications. The measured melting temperature of LA was -5.6°C, which is very close to the reported value -5 °C [130].

Finally, the SODD presented two characteristic peaks in crystallization and melting cycles. These peaks are less sharp compared to those of the other fatty acids under study, which can be attributable to their higher content of acylglycerides. The SODD exhibited two crystallization events at 8.38°C and -34°C, and two melting peaks at -23.7°C and 19.7°C, respectively. Such behavior is consistent with the high content of oleic and linoleic acid. Also, the thermal behavior of SODD is highly dependent of other compounds present in the mixture such as acylglycerides, tocopherols, squalene, phytosterols, and soaps.

In terms of thermal degradation, pure fatty acids such as oleic and linoleic acid, exhibited a single degradation stage near 346°C. In contrast, SODD has two degradation peaks at 331.3 and 415.7°C. This is consistent with the high content of unsaturated fatty acids and other high molecular weight components in the feedstock.

- Procedure

Esters of isobutanol, namely isobutyl oleate (IBO), isobutyl linoleate (IBL), and isobutyl soyate (ISO), were obtained via Fisher esterification of fatty acids and isobutanol using sulfuric acid as a catalyst in an inert nitrogen atmosphere. The esterification reaction was carried out in a 150 ml glass four-necked jacketed reactor equipped with a thermometer, a magnetic agitator, and a continuous heating fluid flow from a thermostatic bath (MV-4, Julabo). The system also featured a vigreux column, a condenser, and a cylindrical separatory funnel to recover condensates. The experimental setup for the esterification reaction is illustrated in Figure 3-6.

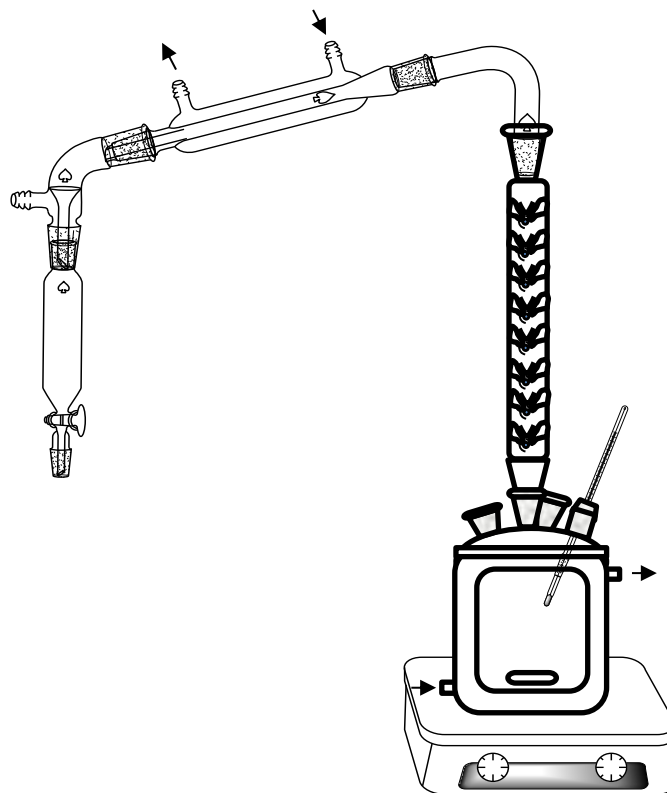


Figure 3-6. Experimental setup during esterification experiments

All esterification experiments were performed under a stirring rate of 650 rpm and 94°C of temperature at the local pressure of 74.6 kPa. Two different reaction conditions were used: 3:1 molar ratio of isobutanol to a fatty acid, 1% wt. sulfuric acid as catalyst, and 5:1, 2% wt. catalyst. Fatty acids were heated up until the reaction temperature was reached. Then a mixture of catalyst and isobutanol was dosed to the reactor. After 20 minutes, some water and isobutanol were evaporated, condensed, and recovered in the side cylindrical collector. The top vapor temperature reached a maximum of 80 °C before the temperature profile dropped. As expected due to the large excess of isobutanol, and the liquid-liquid equilibrium of the system presented in Figure 3-1 [143], the condensed vapor underwent a liquid-liquid splitting. According to the phase equilibria, at the temperature of the condensate (~293K) the heavy phase was mainly composed of water (~ 92% wt.), and the light phase was mainly composed of isobutanol (~ 84% wt. isobutanol).

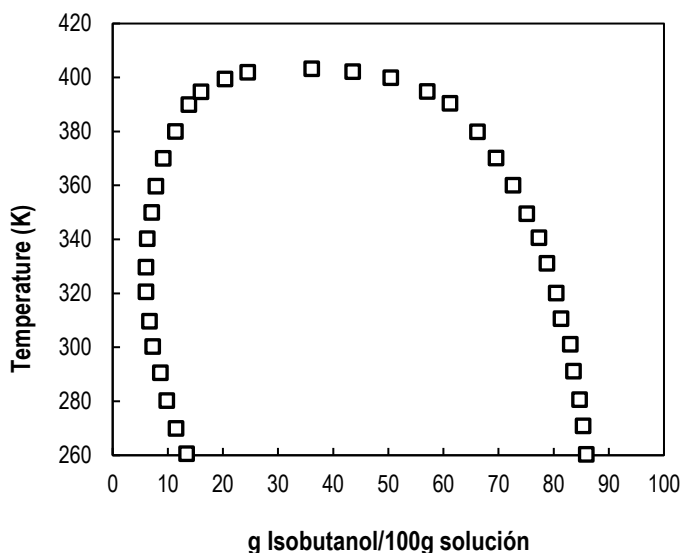


Figure 3-7. Liquid – Liquid Equilibrium for the mixture isobutanol-water

Adapted from [134]

Samples of 1g were extracted at different time intervals during the reaction, and the progress of esterification was monitored by measuring the acid value. After 6 hours, the reaction mixture containing the ester, the acid catalyst, and the residual alcohol was neutralized using 80% of the required stoichiometric amount of a saturated NaOH solution in isobutanol, followed by vacuum distillation. The mixture was then neutralized again until the acid value was lower than 0.06 mg KOH/g. Then the solution was washed with water until pH 7 and dried under vacuum. The neutralization of the remaining fatty acids in the reaction medium was slow due to the low solubility of NaOH in isobutanol. However, alcoholic neutralization in the absence of water reduced soap formation and facilitated separation processes.

- Esterification kinetics

The conversion of the esterification reaction was monitored by measuring the acid value along the reaction time. The conversion is expressed as follows:

$$X = \frac{W_{FFA}(t)}{W_{FFA}(t_0)} * 100 \quad (3-2)$$

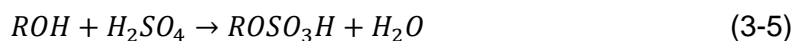
In Equation (3-2), $N_{FFA}(t)$ is the mass of fatty acid at time (t) and $W_{FFA}(t_0)$ is the initial mass of fatty acid. Using the definition of acid value, this equation can be written as:

$$X = \frac{VA_t(t) * w_t - VA_{H_2SO_4} * w_{H_2SO_4}}{VA_r(t_0) * w_r} \quad (3-3)$$

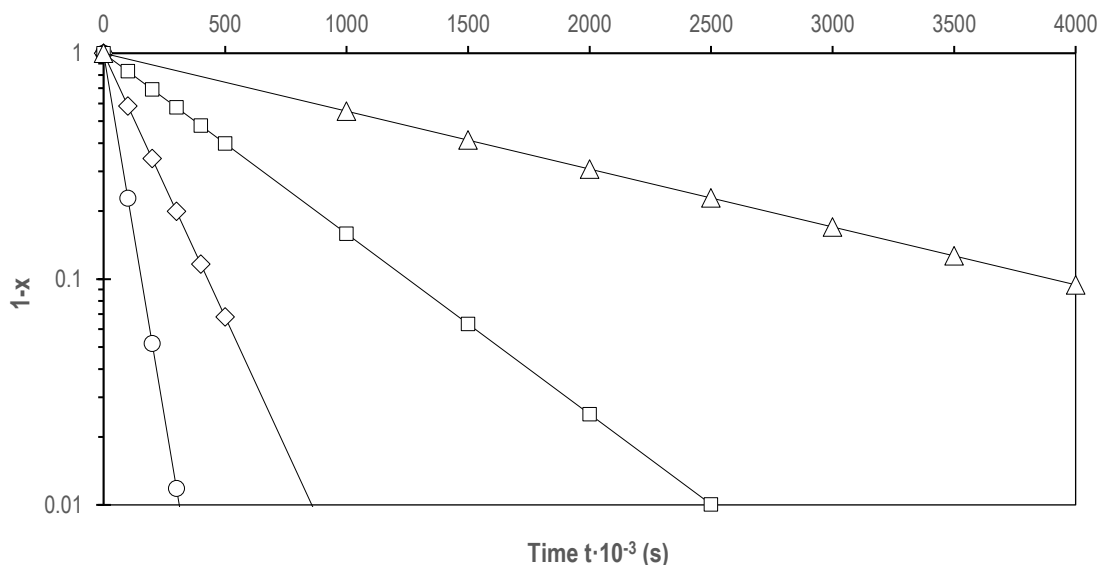
In Equation (3-3), $VA_r(t_0)$ and w_r are the initial acid value of the fatty acid in the reactor and the initial mass of the FFA. $VA_{H_2SO_4,r}$ is the acid value of sulfuric acid and $w_{H_2SO_4}$ is its weight in the reactor mixture. $VA_r(t)$ is the acid value in the reactor along the time and w_t is the corresponding mass of the reactor mixture at sampling time t. Assuming that the total mass of fatty acids in the reactor was constant (negligible change by evaporation or by samples withdrawal) and that the total acid content in the condensate was negligible (< 0.54 mg KOH/g), Equation(3-3) can be rewritten as:

$$X = \frac{VA_r(t) - VA_{H_2SO_4,r}}{VA_r(t_0)} \quad (3-4)$$

By using this Equation, conversion along reaction was monitored for 3 hours. However, from initial calculations of acid values, it was possible to verify that a secondary reaction was occurring. At high conversions, the acid equivalents of the sulfuric acid catalyst in the reactive media resulted lower than the initially loaded ones. According to previous reports [144],[145], the inorganic acid catalysts can sulfate the alcohol to produce an alkyl sulfuric acid ($ROSO_3H$). The sulfation reaction between isobutyl alcohol and sulfuric acid is depicted in Equation (3-5).



In the reported studies, it was found that monovalent isobutyl sulfuric acid was produced irreversibly during the esterification process, and its formation could reduce the acid value of the catalysts to half of the initial acidity at all tested temperatures (57 to 87°C) and alcohol to acid molar ratios (i.e. 10^2 of to 10^3). Figure 3-10 illustrates the observed conversions during the reaction, as reported in the aforementioned studies [145].



(-○-) 360K. (-◇-) 350K. (-□-) 340K. (-Δ-) 330K reported by [145]
Figure 3-8. Sulfuric acid concentration with reaction time.

To evaluate the variation of the inorganic acidity due to the side reaction, isobutanol, and sulfuric acid were reacted in the absence of fatty acids. The two experiments were run at 1.3 and 1.5% wt. sulfuric acid in isobutanol with a molar ratio sulfuric acid: isobutanol of 104 and 87 respectively. The mixture was heated to 94°C at 650 rpm under reflux in a flask equipped with a condenser, a thermometer, and a magnetic stirrer. Aliquots of 1 g were withdrawn at different time intervals and the acid value was measured. In this case, the acid value was equivalent to the sum of the acidity of sulfuric acid and monovalent isobutyl sulfuric acid [145]. The conversion of the side reaction using a 1.3% wt. sulfuric acid in the alcohol is presented in Figure 3-8, and the results from both experiments are summarized in Table 3-4. As observed, the side reaction is almost complete within the first five minutes. Similar results were obtained for the case of a 2% wt. sulfuric acid loading. As a result, the acid value of the catalyst decreased by 41 and 45% respectively for each reaction condition.

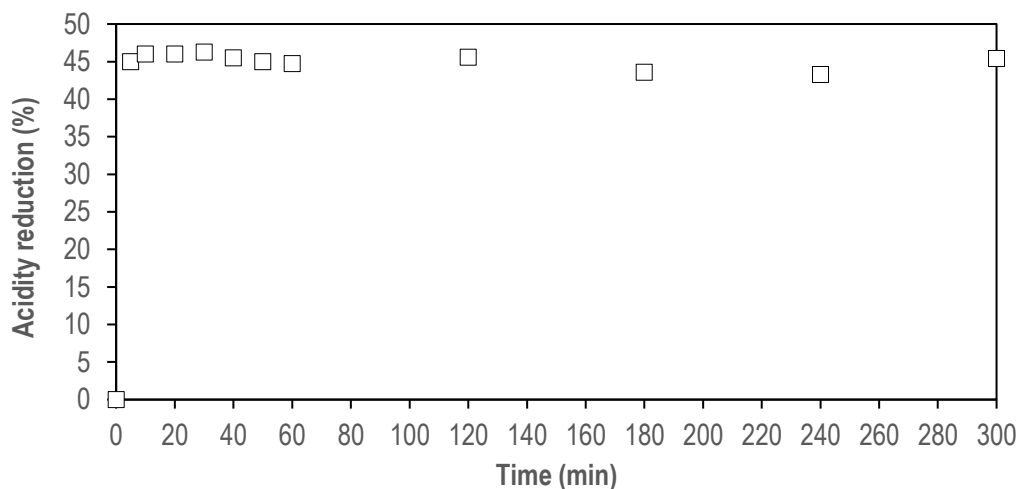


Figure 3-8. Reduction of acidity during sulfation of isobutyl alcohol under 1% wt. of sulfuric acid at 94°C

Table 3-4. Operating conditions and results during sulfation of isobutanol with sulfuric acid

| Reaction conditions | | | Acid value reduction (%) |
|---------------------|------|--------------|--------------------------|
| % Catalyst | °T | Ratio OH:FFA | |
| 2% | 94°C | 5:1 | 41.1 ± 3 |
| 1% | 94°C | 3:1 | 45.2 ± 1 |

The obtained results were similar to those observed in previous studies. At higher temperatures (above 340K) the acid value decreased with time and achieved a constant value within an hour of reaction. Then, it was verified that the side reaction of isobutyl alcohol and sulfuric produces a significant reduction of the acid value of the catalyst. The experimental reduction of the acidity as reported in Table 3-4 and the mass balance of the system were used to correct the calculated acid value along reaction time (i.e. $VA_r(t)$). The conversion of the esterification was then computed according to Equation (3-4). The conversion of the esterification reaction of oleic acid, linoleic acid, and SODD over time are presented in Figure 3-9, Figure 3-10, and Figure 3-11, respectively. Table 3-5 presents the final conversion of each fatty acid.

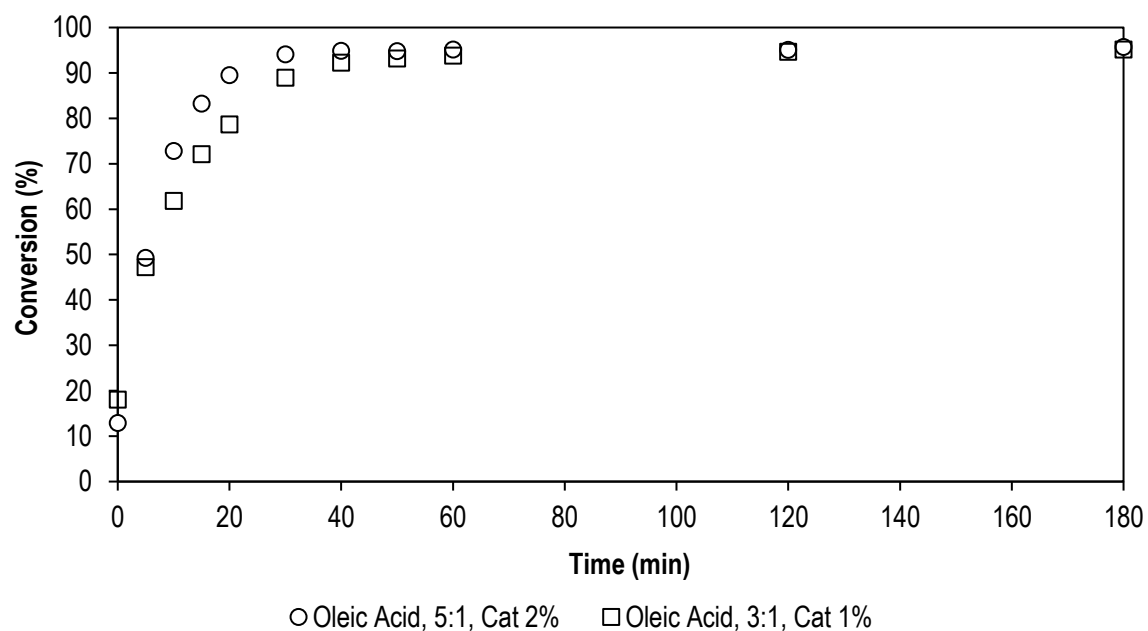


Figure 3-9. Esterification of oleic acid with isobutanol at 94°C

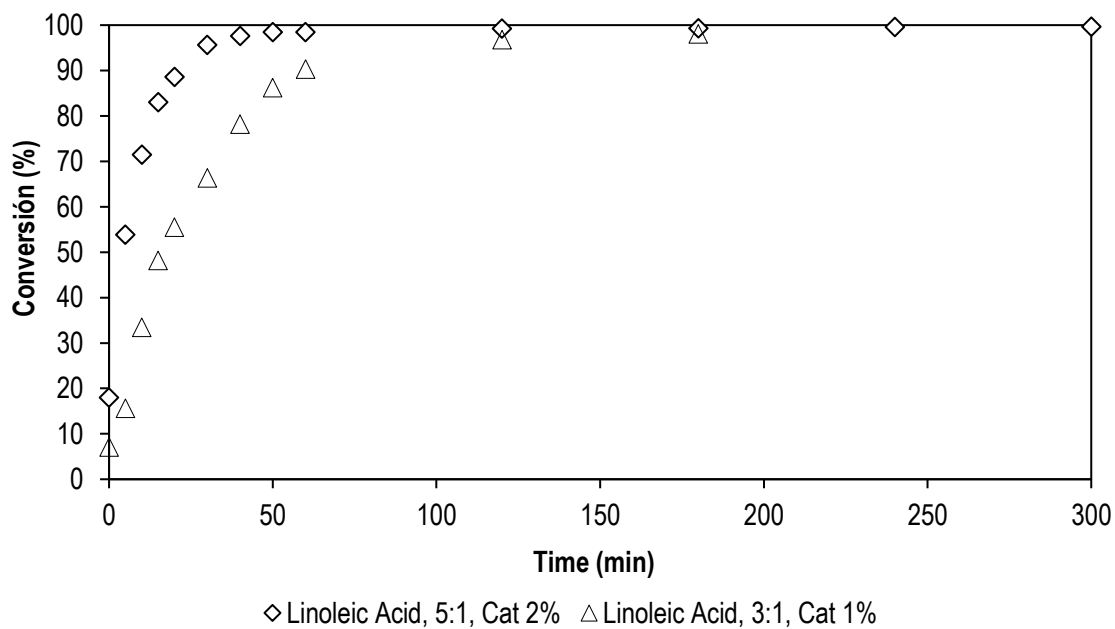


Figure 3-10. Esterification of linoleic acid with isobutanol at 94°C

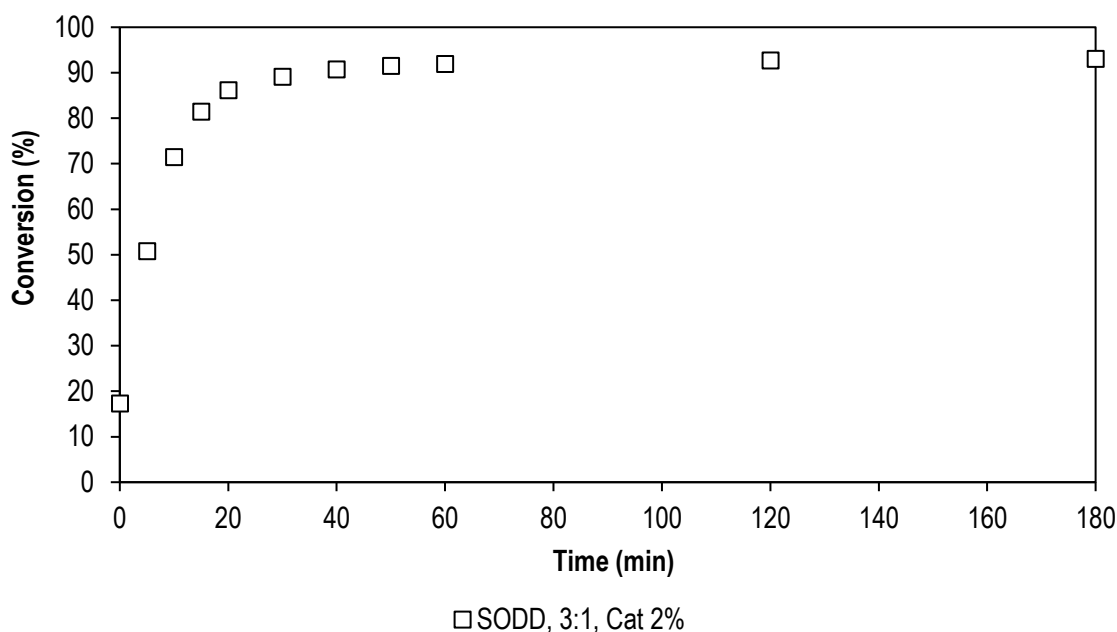


Figure 3-11. Esterification of SODD with isobutanol at 94°C

Table 3-5. Final conversion of fatty acids by esterification with isobutanol

| Fatty Acid | Ratio 5:1, Cat 2% | Ratio 3:1, Cat 1% | Ratio 3:1, Cat 2% |
|---------------|-------------------|-------------------|-------------------|
| Linoleic Acid | 99.7 | 98.0 | -- |
| Oleic Acid | 96.4 | 96.2 | -- |
| SODD | -- | -- | 93.0* |

* Based on the acid content

High conversions were obtained for the esterification of oleic acid and linoleic acid, ranging from 99 to 96%, by removing the water produced during the ester formation. Similar conversions were achieved in reference works [146],[147]. Regarding the SODD, a 93% conversion was achieved based on its acid content. As mentioned above, this feedstock contains glycerides and unsaponifiable material that affect the esterification kinetics and can consume the acid catalyst. To obtain a purer ester from SODD, isobutyl soyate (ISO) was distilled under vacuum to remove undesired compounds.

- Distillation of Isobutyl soyate (ISO)

The obtained Isobutyl soyate (ISO) was distilled in a 150 ml two-necked jacketed flask equipped with a thermometer, a magnetic agitator, and a condenser. The system was

coupled to a high vacuum pressure pump and a thermostatic bath (MV-4 Julabo) for circulation of the cooling fluid. The distillation was performed at 180°C and 0.1 mbar. The first drop of distillate was obtained at a head temperature of 118°C, and after this point, the temperature gradually raised until it reached 178°C at the end of the distillation. The complete set of temperatures observed during vacuum distillation is presented in Table 3-6. According to the observed behavior, it can be inferred that the boiling point of isobutyl soyate at 0.1 mbar is around 118°C. According to the mass balance, the target distillation fraction was 0.45 of the feed.

Table 3-6. Observed temperatures during isobutyl soyate distillation.

| Boiling temperature (°C) | Head temperature (°C) |
|--------------------------|-----------------------|
| 180 | 118 |
| 180 | 124 |
| 180 | 144 |
| 180 | 162 |
| 182 | 164 |
| 183 | 166 |
| 185 | 178 |

Based on the fatty acid composition of the SODD presented in Table 1-1 and Table 3-2, it is expected that the major components of the distillate product were fatty acid esters of C16 chains and fractions of C18:0, C18:1, C18:2, C18:3. On the other hand, it would be expected that major components in the bottoms were fatty acid esters of C18:0 and minor fractions of C16, C18:1, C18:2, C18:3. Distilled isobutyl soyate (ISD) was recovered and used together with the other esters, namely isobutyl oleate (IBO), isobutyl linoleate (IBL), isobutyl soyate (ISO), in subsequent epoxidation process.

- Characterization of the esters

The results from the physicochemical characterization of the obtained esters are summarized in Table 3-7, and the appearance of such products can be observed in Figure 3-12. All esters exhibited low acid values (< 0.5 mg KOH/g) and iodine values above 102 I₂/100g, which is desirable for the epoxidation process. According to these values, the maximum theoretical oxirane content in the epoxidized isobutyl esters of IBO, IBL, ISD, and ISO would be 6.0, 8.4, 6.1, and 6.4% wt., respectively. Concerning the unsaturation content, the average instauration of isobutyl oleate and isobutyl linoleate were 1.4 and 1.9

respectively. The molecular weight of IBO and IBL was calculated based on the saponification value, but this parameter is not presented for ISD and ISO since these esters have an unknown mixture of glycerides. Finally, because of the esterification process, the density and viscosity of the isobutyl esters decreased compared to those obtained for the feedstocks.

Table 3-7. Results characterization of isobutyl esters

| Parameter | IBO | IBL | ISD | ISO |
|---|-----------------|-----------------|-----------------|----------------|
| Acid value (mg KOH/g) | 0.41 ± 0.02 | 0.3 ± 0.1 | 0.4 ± 0.1 | 0.3 ± 0.1 |
| Iodine value (g I ₂ /100g) | 101.1 ± 0.5 | 146.3 ± 0.7 | 102.9 ± 0.3 | 108 ± 0.2 |
| Saponification value (mg KOH/g) | 166.5 ± 0.6 | 165.3 ± 0.2 | 139.4 ± 0.1 | 126 ± 1 |
| Density (20°C) (kg/m ³) | 871.4 | 874.8 | 869.5 | 882.5 |
| Density (40°C) (kg/m ³) | 853.4 | 856.8 | 853.5 | 864.5 |
| Kinematic Viscosity (40°C) (cSt) | 6.43 ± 0.03 | 5.20 ± 0.06 | 5.72 ± 0.07 | 8.7 ± 0.2 |
| Dynamic Viscosity (40°C) (cP) | 5.49 ± 0.03 | 4.45 ± 0.06 | 4.88 ± 0.07 | 7.57 ± 0.2 |
| Color | Yellow | Orange | Yellow | Brown |
| Calculated | | | | |
| Calculated MW (g/mol) | 337.7 | 340.0 | -- | -- |
| II theoretical (g I ₂ /100g) | 106.3 | 148.7 | -- | -- |
| reported MW (g/mol) | 338.60 | 336.55 | -- | -- |
| Average instaurations | 1.4 | 1.9 | -- | -- |



a) b) c) d)

Figure 3-12. Appearance of the obtained isobutyl esters.

a) Isobutyl Oleate b) Isobutyl Linoleate c) Distilled isobutyl soyate d) isobutyl soyate

- Thermal properties of esters

To study the thermal properties of the esters (IBO, IBL, ISD, and ISO), the samples were analyzed using the same thermal cycles (crystallization and melting), that were employed to evaluate the thermal properties of free fatty acids. The crystallization and melting cycles of isobutyl esters are shown in Figure 3-13 and Figure 3-14, and the thermal degradation of these esters is presented in Figure 3-15.

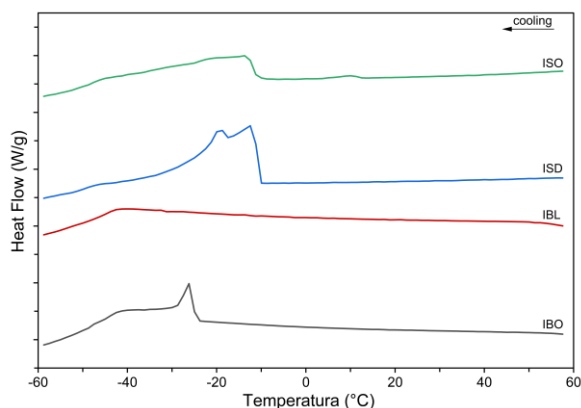


Figure 3-13. Crystallization DSC curves of isobutyl esters

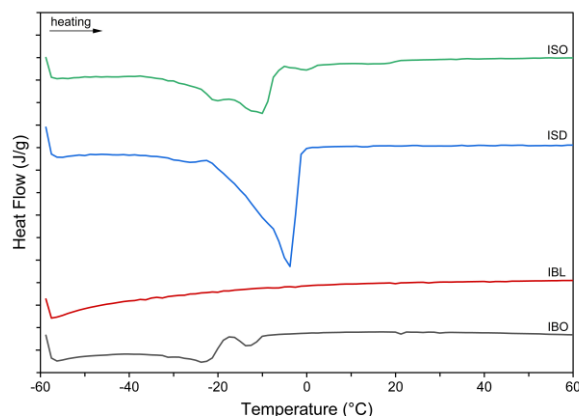
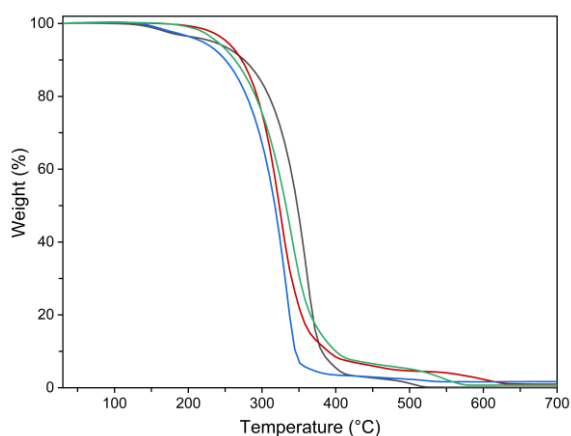


Figure 3-14. Melting DSC curves of isobutyl esters



(— IBO) (— IBL) (— ISD) (— ISO)

Figure 3-15. Thermal degradation of isobutyl esters

According to the obtained calorimetric profiles, the crystallization temperatures of isobutyl esters were -26.3, -13.5, and -11.9 °C for IBO, ISO, and ISD, respectively. The melting temperatures were -22, -9.8 and 3.9 °C for IBO, ISO, and ISD, respectively. Regarding the thermal properties of isobutyl linoleate, it is very likely that these values were outside the

range of measurement since no attenuated peaks were found in both cycles. As expected, the isobutyl esters exhibited lower crystallization and melting temperatures than those obtained for the FFA, showing a more liquid-like behavior. This is because the introduction of an ester group of a branched alcohol increases intermolecular distances and hinders their interactions. Regarding degradation temperatures of the esters, they remained similar to those of the fatty acids. This might indicate that degradation initially occurs in the same type of moieties that are present in both molecules, namely the unsaturation of the fatty acid chain. However, the IBL presented a slight decrease of around 13°C of this parameter.

3.3 Epoxidation

According to the context developed in Chapter 1, three variables were selected for the kinetic study during the epoxidation step: temperature, molar ratio of H_2O_2 , and Acetic acid (AA) to unsaturation content. The epoxidation kinetic study was performed only using isobutyl linoleate, as this was the only ester of well-defined nature. As identified in previous works [85],[148], optimal epoxidation yields are obtained in the following range of conditions; temperature: 50-80 °C, catalyst loading 1-2% wt., and molar ratio $\text{C}=\text{C}/\text{AA}/\text{H}_2\text{O}_2$ 1:0.5:2. Hence, these conditions were selected for the experiment design. Additionally, a stirring rate of 600 rpm was used to maintain a well-mixed reactive medium and a suitable temperature control. It has been reported that operating between stirring rates of 300 and 900 rpm, neither mass transfer limitations nor significant differences in the epoxide content during the reaction are present [84],[95].

- Box Behnken design for the epoxidation reaction

The effect of the variables on the epoxidation process was studied through a Box Behnken design of 3 variables and 3 levels. The parameters considered were temperature, molar ratio $\text{AA}:\text{C}=\text{C}$, and molar ratio $\text{C}=\text{C}:\text{H}_2\text{O}_2$. Furthermore, three additional runs were proposed to evaluate the effect of the catalyst loading and temperature. The complete set of conditions of all experiments is presented in Table 3-8. The reaction progress was monitored by measuring the oxirane oxygen content and iodine value. The main response variables were the conversion of double bonds, epoxide yield, and selectivity.

Table 3-8. Box Behnken experimental design

| Run | Factors | | | | | | Catalyst (% wt.) | Run |
|-----|----------------|----------------|----------------|---------|--------------|---|---------------------|-----|
| | X ₁ | X ₂ | X ₃ | °T (°C) | Ratio AA:C=C | Ratio C=C:H ₂ O ₂ | | |
| 1 | -1 | -1 | 0 | 50 | 0.3 | 1.5 | 2.0 | L10 |
| 2 | 1 | -1 | 0 | 70 | 0.3 | 1.5 | 2.0 | L14 |
| 3 | -1 | 1 | 0 | 50 | 0.5 | 1.5 | 2.0 | L11 |
| 4 | 1 | 1 | 0 | 70 | 0.5 | 1.5 | 2.0 | L15 |
| 5 | 0 | 0 | 0 | 60 | 0.4 | 1.5 | 2.0 | L8 |
| 6 | 0 | -1 | -1 | 60 | 0.3 | 1 | 2.0 | L7 |
| 7 | 0 | -1 | 1 | 60 | 0.3 | 2 | 2.0 | L6 |
| 8 | 0 | 1 | -1 | 60 | 0.5 | 1 | 2.0 | L5 |
| 9 | 0 | 1 | 1 | 60 | 0.5 | 2 | 2.0 | L4 |
| 10 | 0 | 0 | 0 | 60 | 0.4 | 1.5 | 2.0 | L2 |
| 11 | -1 | 0 | -1 | 50 | 0.4 | 1 | 2.0 | L13 |
| 12 | -1 | 0 | 1 | 50 | 0.4 | 2 | 2.0 | L12 |
| 13 | 1 | 0 | -1 | 70 | 0.4 | 1 | 2.0 | L16 |
| 14 | 1 | 0 | 1 | 70 | 0.4 | 2 | 2.0 | L17 |
| 15 | 0 | 0 | 0 | 60 | 0.4 | 1.5 | 2.0 | L9 |
| 16 | 0 | 1 | 0 | 80 | 0.5 | 1.5 | 2.0 | L18 |
| 17 | 0 | 0 | 0 | 60 | 0.4 | 1.5 | 1.0 | L1 |
| 18 | 0 | 0 | 0 | 60 | 0.4 | 1.5 | 1.5 | L3 |

L1, L3 and L18 were carried out using variable catalyst and L18 was performed at a higher temperature (80°C)

- Procedure

Epoxidized isobutyl linoleate (EIL) was produced by epoxidation of isobutyl linoleate using peracetic acid generated in situ, and sulfuric acid as a catalyst. The reaction was carried out in a 150 ml glass five-necked jacketed and coiled reactor equipped with a thermometer, and a mechanical stirrer. The reactor was connected to two thermostatic baths, one to provide heating and the other to provide cooling circulating fluids. The immersed coil was used to remove the heat of the reaction, and the jacket was used to maintain the reaction temperature. The system was provided with a calibrated syringe pump to dose the H₂O₂ feed and a reflux condenser to recover the volatile species. The experimental setup for the epoxidation reaction is presented in Figure 3-16.

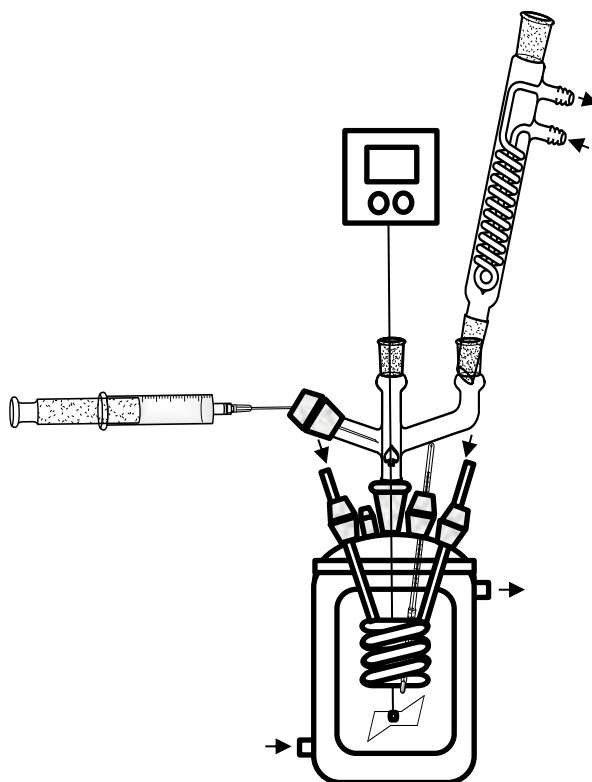


Figure 3-16. Experimental setup used during epoxidation of fatty esters.

In the setup, 70 g of isobutyl linoleate and the corresponding amount of acetic acid, according to the experiment design, were added to the reactor and heated up to the reaction temperature. A mixture of sulfuric acid and aqueous hydrogen peroxide was then added dropwise to the reactor over a period of 10 minutes. The temperature of the reaction was held isothermal by using a coil connected to a thermostatic bath which refrigerated the reaction medium. Samples of 0.5 g were withdrawn at different time intervals and quenched by immersing the sample holder in cold water to stop the reaction. The reaction progress was monitored by measuring the acid value, iodine value, and oxirane oxygen content in the samples. After 3 hours, the reaction was stopped, and the content of the reactor was removed and transferred to a glass funnel for separation. The water phase was discarded. Subsequently, the oil phase containing the epoxide was neutralized using a 5% wt bicarbonate solution and rinsed with water at 40°C until the aqueous effluent reached a neutral pH. Finally, the epoxide was dried over MgSO_4 to remove the residual water.

3.3.1 Results

The results of the epoxidation study are summarized in Table 3-9. The effect of catalyst loading (1, 2, and 1.5% wt.) was studied at 60°C in runs L1, L2, and L3. The oxirane content achieved in those runs was about 5.1%, and the conversions were 73%, 81 and 88.6%, respectively. Nevertheless, the highest selectivity was reached using 1% wt. catalyst. As expected, high catalyst concentrations also trigger ring-opening reactions in the presence of water and decrease the yield of the reaction [86],[94],[147].

Table 3-9. Run results and reaction conditions.

| Run | °T(°C) | Ratio C=C: CA: H ₂ O ₂ | Catalyst (%) | II (gl ₂ /100g) | OO (%) | Y (%) | X (%) | S (%) |
|-----|--------|---|-----------------|----------------------------|-----------|----------|----------|----------|
| L1 | 60 | 1 : 0.4 : 1.5 | 1.0 | 40.2 | 5.0 | 58.9 | 72.5 | 81.2 |
| L2 | 60 | 1 : 0.4 : 1.5 | 2.0 | 16.6 | 5.1 | 60.3 | 88.6 | 68.0 |
| L3 | 60 | 1 : 0.4 : 1.5 | 1.5 | 27.7 | 5.1 | 60.6 | 81.1 | 74.8 |
| L4 | 60 | 1 : 0.5 : 2.0 | 1.4 | 16.7 | 5.2 | 61.6 | 88.6 | 69.5 |
| L5 | 60 | 1 : 0.5 : 1.0 | 1.6 | 29.1 | 3.8 | 44.8 | 80.1 | 55.9 |
| L6 | 60 | 1 : 0.3 : 2.0 | 2.0 | 16.6 | 5.2 | 61.8 | 88.6 | 69.7 |
| L7 | 60 | 1 : 0.3 : 1.0 | 2.2 | 24.1 | 4.7 | 55.1 | 83.5 | 66.0 |
| L8 | 60 | 1 : 0.4 : 1.4 | 1.9 | 14.6 | 5.0 | 59.4 | 90.0 | 66.0 |
| L9 | 60 | 1 : 0.4 : 1.4 | 1.9 | 16.3 | 5.1 | 60.3 | 88.8 | 67.9 |
| L10 | 50 | 1 : 0.3 : 1.5 | 2.0 | 41.6 | 4.8 | 56.5 | 71.6 | 79.0 |
| L11 | 50 | 1 : 0.5 : 1.5 | 2.0 | 25.3 | 4.9 | 58.6 | 82.7 | 70.8 |
| L12 | 50 | 1 : 0.4 : 2.0 | 2.1 | 30.8 | 5.0 | 59.4 | 78.9 | 75.3 |
| L13 | 50 | 1 : 0.4 : 1.0 | 2.1 | 43.3 | 4.2 | 49.9 | 70.4 | 70.9 |
| L14 | 70 | 1 : 0.3 : 1.5 | 2.0 | 5.3 | 4.7 | 56.0 | 96.4 | 58.1 |
| L15 | 70 | 1 : 0.5 : 1.5 | 2.0 | 4.3 | 0.5 | 6.3 | 97.0 | 6.5 |
| L16 | 70 | 1 : 0.4 : 1.0 | 2.1 | 19.2 | 2.9 | 34.4 | 86.9 | 39.6 |
| L17 | 70 | 1 : 0.4 : 2.0 | 2.0 | 1.5 | 2.6 | 30.7 | 99.0 | 31.0 |
| L18 | 80 | 1 : 0.5 : 1.5 | 2.0 | 5.6 | 0.0 | 0.0 | 96.1 | 0.0 |

Y: yield, X: conversion S: selectivity.

The dependence of epoxidation conversion on the catalyst loading is presented in Figure 3-17. It is possible to verify that final conversion linearly increases with catalyst loading, which is characteristic when using a homogenous catalyst, and mass transfer limitations are absent. In further experiments, a 2% wt. H₂SO₄ loading was used to enable higher reaction rates.

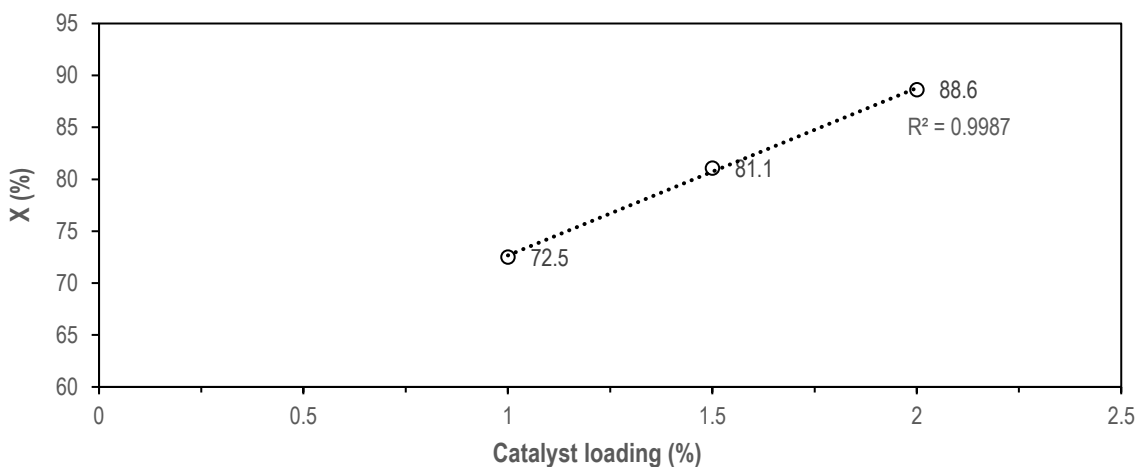


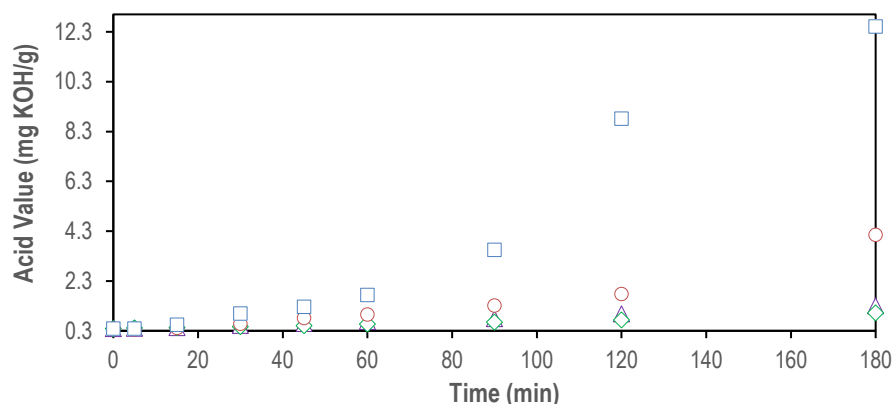
Figure 3-17. Acid homogeneous catalyst loading vs conversion.

The effect of the temperature was studied from 50°C to 80°C. As expected, high temperatures enhance the rate of epoxidation but also have a negative effect on the selectivity and yield to oxirane groups. This is clear when comparing the final concentration of oxirane at 60°C, 70°C, and 80°C, which is almost zero at the highest temperature. Therefore, when the epoxidation is carried out above 60°C, it is necessary to identify the point of maximum oxirane production to quench and stop the reaction [85].

Previous works have reported that degradation reactions are highly dependent on temperature and catalyst loading in the reactive medium [86],[89]. High temperatures and high catalyst concentrations trigger the nucleophilic attack on the oxirane ring at the interphase and the oil phase. In the used epoxidation route, the main nucleophiles are the acetic acid which is partially soluble in the oily phase, and the water which is in large excess. Hydrogen peroxide has low solubility in the oil phase due to its polar nature and tends to react with carboxylic acids, so its oxirane cleavage capacity can be considered negligible. According to these considerations, the most likely degradation reactions are mainly caused by the attack of acetic acid and water over the oxirane ring.

From the epoxidation results in Table 3-9, it is observed that the increasing of the molar ratio of hydrogen peroxide increases the rate of epoxidation (runs L4 and L5). However, a large loading of aqueous H_2O_2 also increases the content of water in the reaction medium up to a level where its concentration is 4 to 8 times that of acetic acid. Besides becoming a

major issue for oxirane ring stability, an excess of water under acidic conditions can promote hydrolysis of the ester [86]. This was characterized during epoxidation experiments, and Figure 3-18 shows the measured acid value of the reactive medium over time. As observed, the acid value increased with the reaction time. At 50°C and 60°C it displayed a slightly linear growth, but acidity exponentially increased when operating at 70°C and 80°C. This trend indicates that the hydrolysis reaction is promoted by the acid catalyst under large water excess and high temperatures.



(-□-) Run L18 - 80°C. (-○-) Run L15 - 70°C. (-△-) Run L7 - 60°C. (-◇-) Run L11 - 50°C.
Figure 3-18. Acid value of the reactive medium along time during epoxidation reactions at different temperatures.

Increasing the molar ratio of acetic acid also has a significant effect on the ring-opening reactions. According to runs L15 and L18, a complete ring opening was attained using a molar ratio of 0.5 at temperatures of 70 and 80°C. This fact, coupled with degradation by water, resulted in the lowest selectivity and yield in these experimental runs.

Conversely, the highest oxirane oxygen 5.2% was reached in runs L6 and L4 at 60°C after 3 hours of reaction. This oxirane content represents a yield of 62% and a conversion of 89%.

In this regard, it can be concluded that moderate oxirane cleavage is achieved at mild conditions, but operating under such conditions hinders the maximum oxirane concentration, which, in the case of isobutyl linoleate, is 8.4%.

Regarding the effect of reaction time, evaluating the oxirane content as a function of time for each run enables to define the highest oxirane production along the reaction. In this case, an oxirane content of 5.5% wt. was achieved using the following reaction conditions: 70°C, 1:0.3:1.5, and 2% wt. catalyst, and 90 min reaction (Run L14). After reaching the maximum oxirane content, it gradually decayed as observed in the kinetic profiles presented in Annex C - L14. Despite a similar yield could also be achieved in runs L10 or L1 at 50°C with a longer reaction time, the conversion of these runs was moderate (~72%) and it was balanced by high selectivity values (~80%). The corresponding selectivity, yield, and conversion of all the experiments are graphically presented in Figure 3-19.

As can be seen, conversions are above 80% in most of the experiments, but selectivity is highly affected by reaction conditions, also impacting the obtained yield. The highest selectivities were obtained in runs L1, L10, and L12. In these runs, the conversion was between 70 – 80%. In this sense, to reach the highest oxirane content, a balance between conversion and selectivity must be achieved [149].

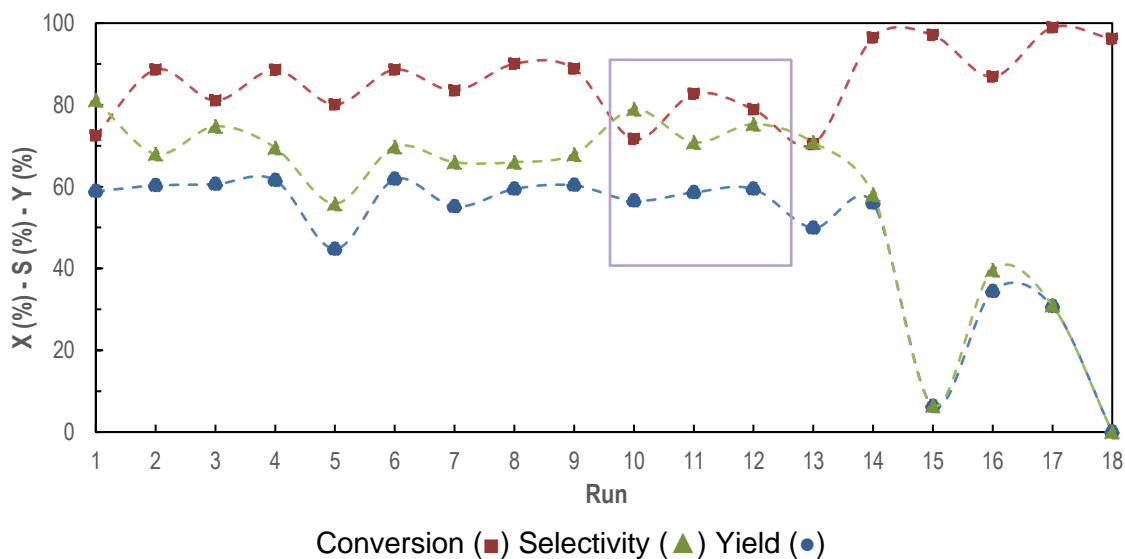
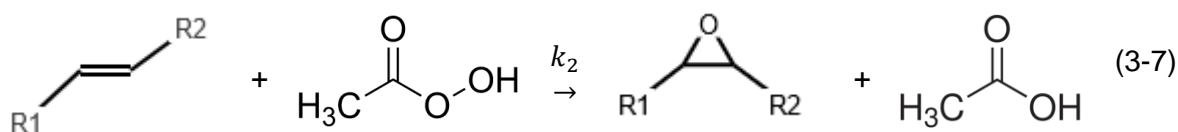
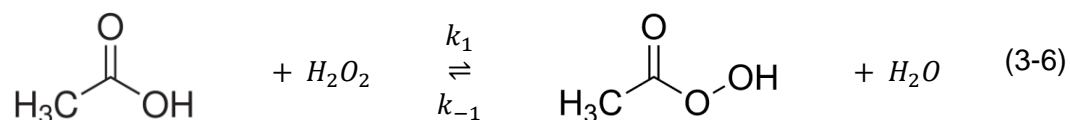


Figure 3-19. Epoxidation results.

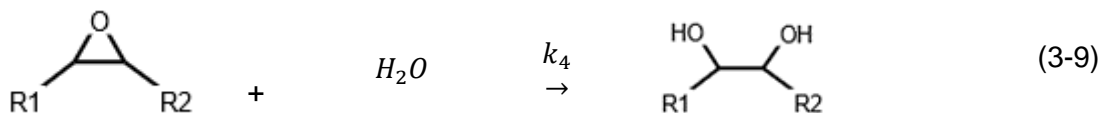
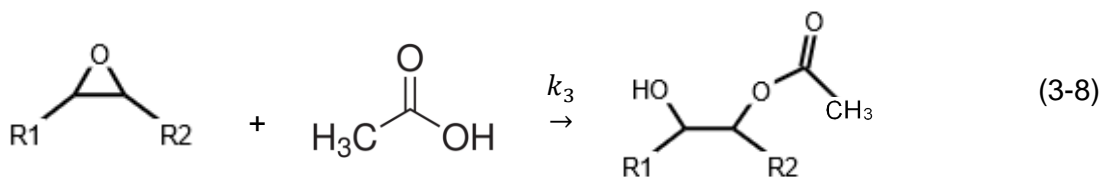
Other degradation reactions, such as H_2O_2 and peracetic acid decomposition, can also decrease the concentration of the reagents and affect the epoxidation rate. However, these reactions were not considered in the present study [87].

3.4 Two-phase epoxidation kinetic model

The epoxidation of unsaturations in which the aqueous and oil phases are well mixed can be modeled using a two-phase reaction system [79],[84],[99]. As is described in Chapter 1, the unsaturation present in the ester molecule reacts with the in situ peracetic acid to produce an oxirane ring, as is shown in Equation (3-6) and Equation (3-7).



The oxirane ring can further react with nucleophilic agents present in the reaction mixture (water, hydrogen peroxide, acetic acid, and peracetic acid) [81]. However, in the modeling of the system, it is assumed that the cleavage of oxirane is only caused by acetic acid and water, as described in Equation (3-8) and Equation (3-9).



Additionally, the kinetic model considers the following assumptions:

- The epoxidation and degradation reactions are irreversible.
- The rate of reaction and mass balances are a function of the molar concentration in each phase and their corresponding volumes.

- Acetic and peracetic are distributed in both phases, while hydrogen peroxide, sulfuric acid, and water are insoluble in the organic phase [150].
- The degradation reactions are carried out at the oil phase (attack by acetic acid) and the liquid-liquid interphase (attack by water) [151], and they are produced by the attack of carboxylic acid and water.
- The mass transfer coefficients for acetic and peracetic acid are equal ($k_{t,PA}a = k_{t,AA}a$)
- The system is isothermal and well-mixed, and mass transfer limitations are negligible.
- The addition of the first drop of the catalyst mixture and aqueous H_2O_2 is considered time zero for the reaction.
- The degradation reaction by acetic acid is assumed to be of second order for acetic acid. On the other hand, the degradation reaction by water is considered of first order for epoxide and water. Likewise, this reaction considers the influence of acid catalyst in the medium. [79],[84],[150] [152].
- Volume and density slightly change along the reaction time.

According to these assumptions, the mass balance of the reaction system is described by first-order differential equations for each component in the aqueous (w) and oil phase (o). The system was modeled as a semi-batch reactor since the mixture of catalyst and hydrogen peroxide was dosed continuously in the first 10 minutes.

- **Mass balance in a semi-batch reactor**

$$\frac{dN_i}{dt} = \sum_{k=1}^4 \vartheta_{i,k} r_{i,k} V^p + F_i \quad (3-10)$$

In this equation, N_i is the total number of moles of component i in the reactor, t is the time coordinate, $r_{i,k}$ is the rate of appearance/disappearance, and $\vartheta_{i,k}$ is the corresponding stoichiometric coefficient of component i in reaction k . V^p is the volume of the corresponding reactive phase p . F_i is the constant feed flow rate of component i during the

initial loading of the reactants and the catalyst. There are four reactions taking place, namely peracetic acid formation and decomposition (r_1 , r_{-1}), isobutyl fatty ester epoxidation (r_2), and ring-opening reactions by acetic acid (r_3) and water (r_4). Rates of reactions are expressed in $\text{mol L}^{-1} \text{min}^{-1}$, and they correspond to equations (3-11) to (3-20). The kinetic models were described as the following power-law expressions:

$$\begin{aligned} r_1 &= k_1 C_{H_2O_2} C_{AA}^W C_{H^+} \\ r_{-1} &= k_{-1} C_{PAA}^W C_{H_2O} C_{H^+} \\ r_2 &= k_2 C_{C=C} C_{PAA}^O \\ r_3 &= k_3 C_{EPO} C_{AA}^O{}^2 \\ r_4 &= k_4 C_{EPO} C_{H_2O} C_{H^+} \end{aligned}$$

Here, $C_{H_2O_2}$ is the concentration of H_2O_2 , C_{AA}^W is the concentration of acetic acid, C_{H^+} is the concentration of the catalyst, C_{PAA}^W is the concentration of peracetic acid, and C_{H_2O} is the concentration of water, all in the aqueous phase. On the other hand, C_{AA}^O is the concentration of acetic acid, C_{PAA}^O is the concentration of peracetic acid, $C_{C=C}$ is the concentration of the isobutyl ester, and C_{EPO} is the concentration of the epoxidized ester, all in the oily phase. The model depends on the following parameters: peracetic forward and backward kinetic constant k_1 , k_{-1} , ($\text{L}^2 \text{mol}^{-2} \text{min}^{-1}$), epoxidation kinetic constant k_2 , ($\text{L mol}^{-1} \text{min}^{-1}$), kinetic constants for the degradation products k_3 ($\text{L}^2 \text{mol}^{-2} \text{min}^{-1}$), k_4 ($\text{L}^2 \text{mol}^{-2} \text{min}^{-1}$), partition coefficients of acetic acid (K_{AA}) and peracetic acid (K_{PAA}), mass transfer coefficients: $k_{t,PAA}a = k_{t,AA}a = k_m a$, (min^{-1}), and phases volume V^W and V^O (L). The resulting material balances of all species are on a molar basis (mol/time). N_{DEG1} corresponds to the degradation product from the ring-opening reaction by acetic acid (r_3), and N_{DEG2} is the degradation product generated from the ring-opening reaction by water (r_4).

Aqueous phase

- Hydrogen peroxide (H_2O_2):

$$\frac{dN_{H_2O_2}}{dt} = F_{H_2O_2} + (-k_1 C_{H_2O_2} C_{AA}^W C_{H^+} + k_{-1} C_{PAA}^W C_{H_2O} C_{H^+}) V^W \quad (3-11)$$

- Peracetic acid (PAA):

The peracetic acid, as well as acetic acid, is distributed between the two phases, thus the mass balance equation includes the mass transfer rate. The mass transfer is described as the flux of the component between phases: $N_A = k_m a (c_A - c_A^*)$. According to the two-film theory, phase equilibrium is achieved at the interface and c_A^* is the composition of the oil that is in equilibrium with the bulk liquid and is equal to $K_{PAA} C_{PAA}^W$.

$$\frac{dN_{PAA}^W}{dt} = (k_1 C_{H_2O_2} C_{AA}^W C_{H^+} - k_{-1} C_{PAA}^W C_{H_2O} C_{H^+}) V^W - k_m a (K_{PAA} C_{PAA}^W - C_{PAA}^O) V^O \quad (3-12)$$

- Acetic acid (AA):

$$\frac{dN_{AA}^W}{dt} = (-k_1 C_{H_2O_2} C_{AA}^W C_{H^+} + k_{-1} C_{PAA}^W C_{H_2O} C_{H^+}) V^W + k_m a (C_{AA}^O - K_{AA} C_{AA}^W) V^O \quad (3-13)$$

- Water (H₂O):

$$\frac{dN_{H_2O}}{dt} = F_{H_2O} + (k_1 C_{H_2O_2} C_{AA}^W C_{H^+} - k_{-1} C_{PAA}^W C_{H_2O} C_{H^+}) V^W - k_4 C_{EPO} V^O \quad (3-14)$$

Oil phase

- Unsaturations (C=C)

$$\frac{dN_{C=C}}{dt} = -(k_2 C_{C=C} C_{PAA}^O) V^O \quad (3-15)$$

- Epoxide (EPO):

$$\frac{dN_{EPO}}{dt} = (k_2 C_{C=C} C_{PAA}^O - k_3 C_{EPO} C_{AA}^{O^2} - k_4 C_{EPO}) V^O \quad (3-16)$$

- Peracetic acid (PAA)

$$\frac{dN_{PAA}^O}{dt} = -(k_2 C_{C=C} C_{PAA}^O) V^O + k_m a (K_{PAA} C_{PAA}^W - C_{PAA}^O) V^O \quad (3-17)$$

- Acetic acid (AA)

$$\frac{dN_{AA}^O}{dt} = (k_2 C_{C=C} C_{PAA}^O - k_3 C_{EPO} C_{AA}^{O^2}) V^O - k_m a (C_{AA}^O - K_{AA} C_{AA}^W) V^O \quad (3-18)$$

- Degradation products from epoxide (N_{DEG1})

$$\frac{dN_{DEG1}^O}{dt} = (k_3 C_{EPO} C_{AA}^O)^2 V^O \quad (3-19)$$

- Degradation products from epoxide (N_{DEG2})

$$\frac{dN_{DEG2}^O}{dt} = (k_4 C_{EPO} C_{H_2O} C_{H^+}) V^O \quad (3-20)$$

The flow of catalyst and hydrogen peroxide is modeled in a time interval of 10 minutes.

$$F_i = \frac{\dot{F}^* x_i}{PM_i} \quad t \leq t_a \quad (3-21)$$

$$F_i = 0 \quad t \leq t_a$$

In Equation (3-21), PM_i and x_i are the molar mass and the mass fraction of the components of the mixture, respectively.

The partition coefficient K_i is denoted as follows [150]:

$$K_i = \frac{C_i^{O*}}{C_i^{W*}} = \frac{N_i^O/V^O}{N_i^W/V^W} \quad (3-22)$$

Here, C_i^O and C_i^W are the molar concentration in the oil phase and the aqueous phase of component i , respectively.

$$N_i = N_i^O + N_i^W \quad (3-23)$$

Using Equation (3-22), the molar mass of the phases can be written as a function of the partition coefficients and the volume of the phases:

$$N_i^O = \frac{K_i V^O N_i}{V^W + K_i V^O} \quad (3-24)$$

$$N_i^W = \frac{V^W N_i}{V^W + K_i V^O} \quad (3-25)$$

Then, the total volume of the phases can be expressed as:

$$V^W = V_{H_2O} + V_{H_2O_2} + V_{AA}^W + V_{PAA}^W + V_{H_2SO_4} \quad (3-26)$$

$$V^O = V_{AA}^O + V_{PAA}^O + V_{EPO} + V_{ES} + V_{DEG1} + V_{DEG2} \quad (3-27)$$

Likewise, the density of the phases can be expressed as:

$$\rho^W = \frac{W_{H_2O} + W_{H_2O_2} + W_{AA}^W + W_{PAA}^W + W_{H_2SO_4}}{V^W} \quad (3-28)$$

$$\rho^O = \frac{W_{AA}^O + W_{PAA}^O + W_{EPO} + W_{ES} + W_{DEG1} + W_{DEG2}}{V^O} \quad (3-29)$$

In addition to these variables, the modified Arrhenius equation is used to correlate a kinetic constant $k(T)$ with the activation energy Ea and preexponential factor A_{prex} [153]. The selected reference temperature was 70°C.

$$k(T) = \exp \left[A + B \left(\frac{T - T_{ref}}{T} \right) \right] \quad (3-30)$$

$$A = \ln(k_{ref}) \quad (3-31)$$

$$B = \frac{Ea}{RT_{ref}} \quad (3-32)$$

$$A_{prex} = \frac{k_{ref}}{\exp \left(-\frac{Ea}{RT_{ref}} \right)} \quad (3-33)$$

In Equations (3-30) to (3-33), A and B are the constants of the modified Arrhenius equation. Ea and A_{prex} are the activation energy and the preexponential factor, respectively.

3.4.1 Kinetic parameters regression

The modeling of the epoxidation reaction was performed using *MATLAB 2022a* and the operating conditions of the 18 experimental runs. The system of differential equations described from (3-11) to (3-20) was solved by numerical integration using the multistep solver *ode15s*, based on differential-algebraic equations (DAEs). The objective function in Equation (3-38) was minimized and corresponds to the difference between experimental values (Equations (3-35) and (3-37)) and the predicted values (Equation (3-34) and Equation (3-36)). The minimization problem was solved by adjusting the corresponding kinetics parameters using the Global Search algorithm implemented in Matlab. To determine the number of moles, the molecular weights of the ester and epoxide were

calculated using the saponification and acid values presented in Table 3-7. The molecular weight of the degradation products was obtained from the reaction stoichiometry.

$$[NDB]_{model} = \frac{N_{ES}}{W_{ES} + W_{EPO} + W_{DEG1} + W_{DEG2}} \quad (3-34)$$

$$[NDB]_{exp} = \frac{IN}{2 * Ai} \quad (3-35)$$

In Equations (3-34) and (3-35) NDB is the number of double bonds, IN is the experimental iodine value and Ai is the molecular mass of iodine.

$$[EPO]_{model} = \frac{N_{EPO}}{W_{ES} + W_{EPO} + W_{DEG1} + W_{DEG2}} \quad (3-36)$$

$$[EPO]_{exp} = \frac{OO}{100 * Ao} \quad (3-37)$$

In Equations (3-36) and (3-37) EPO is the number of oxirane groups, OO is the experimental oxirane value (%) and Ao is the molecular mass of oxygen. As mentioned above, the objective function to minimize is described in Equation (3-38), and the corresponding statistical parameters are described in Equations (3-39) to (3-41).

- Objective Function

$$F = \sqrt{\frac{1}{n} \sum_{L=1}^{18} \sum_{n=1}^9 \left[\left(\frac{([NDB]_{exp} - [NDB]_{model})^2}{([NDB]_{exp,max})^2} \right) + \left(\frac{([EPO]_{exp} - [EPO]_{model})^2}{([EPO]_{exp,max})^2} \right) \right]} \quad (3-38)$$

- Standard deviation

$$SD = \sqrt{\frac{(x_{i,cal} - x_{i,exp})^2}{\sum_{i=1}^{NR} NS_i}} \quad (3-39)$$

- Absolute error

$$AE = \frac{1}{\sum_{i=1}^{NR} NS_i} * \sum_{j=1}^{NR} \sum_{k=1}^{NS} (x_{i,cal} - x_{i,exp}) \quad (3-40)$$

In Equations (3-39) to (3-40), NR is the number of runs, and NS_i is the number of samples.

- **Relative Error**

$$E_{rel} = \frac{\sum_{samples} \left| \frac{x_{i,cal} - x_{i,exp}}{x_{i,exp}} \right|}{n \text{ samples}} * 100 \quad (3-41)$$

In equation (3-41) $x_{i,cal}$ is the calculated value and $x_{i,exp}$ is the experimental value.

3.4.2 Results of kinetic model regression

The corresponding kinetic model of the epoxidation of isobutyl linoleate with H_2O_2 was obtained by adjusting 19 parameters while minimizing the objective function described in Equation (3-38) [154]. The fitted kinetic parameters are summarized in Table 3-10 along with the corresponding confidence intervals. Table 3-10 presents other statistical measures of the model regression.

Table 3-10. Fitted kinetic parameters for the epoxidation of isobutyl esters.

| Parameter | Units | Value | Upper limit | Lower limit |
|---------------------|---|----------------------|----------------------|----------------------|
| $E_{A,1}$ | J/mol | $6.11 \cdot 10^4$ | $6.00 \cdot 10^4$ | $6.21 \cdot 10^4$ |
| A_1 | $L^2 \text{ mol}^{-2} \text{ min}^{-1}$ | $5.88 \cdot 10^7$ | $3.82 \cdot 10^7$ | $9.04 \cdot 10^7$ |
| $E_{A,-1}$ | J/mol | $6.63 \cdot 10^4$ | $6.53 \cdot 10^4$ | $6.73 \cdot 10^4$ |
| A_{-1} | $L^2 \text{ mol}^{-2} \text{ min}^{-1}$ | $1.04 \cdot 10^9$ | $7.10 \cdot 10^8$ | $1.52 \cdot 10^9$ |
| $E_{A,2}$ | J/mol | $5.74 \cdot 10^4$ | $5.70 \cdot 10^4$ | $5.78 \cdot 10^4$ |
| A_2 | $L \text{ mol}^{-1} \text{ min}^{-1}$ | $5.96 \cdot 10^8$ | $5.03 \cdot 10^8$ | $7.06 \cdot 10^8$ |
| $E_{A,3}$ | J/mol | $4.00 \cdot 10^4$ | $3.93 \cdot 10^4$ | $4.06 \cdot 10^4$ |
| A_3 | $L^2 \text{ mol}^{-2} \text{ min}^{-1}$ | $8.52 \cdot 10^3$ | $5.91 \cdot 10^3$ | $1.23 \cdot 10^4$ |
| $E_{A,4}$ | J/mol | $9.97 \cdot 10^4$ | $9.79 \cdot 10^4$ | $1.01 \cdot 10^5$ |
| A_4 | $L^2 \text{ mol}^{-2} \text{ min}^{-1}$ | $1.21 \cdot 10^{11}$ | $5.33 \cdot 10^{10}$ | $2.74 \cdot 10^{11}$ |
| $KAA_{50^\circ C}$ | -- | 0.659 | 0.655 | 0.664 |
| $KAA_{60^\circ C}$ | -- | 0.687 | 0.684 | 0.692 |
| $KAA_{70^\circ C}$ | -- | 0.783 | 0.780 | 0.785 |
| $KAA_{80^\circ C}$ | -- | 0.892 | 0.808 | 0.975 |
| $KPAA_{50^\circ C}$ | -- | 0.442 | 0.378 | 0.506 |
| $KPAA_{60^\circ C}$ | -- | 0.490 | 0.467 | 0.512 |
| $KPAA_{70^\circ C}$ | -- | 0.704 | 0.641 | 0.767 |
| $KPAA_{80^\circ C}$ | -- | 0.848 | 0.771 | 0.924 |
| $kt \cdot a$ | min^{-1} | 24.46 | 24.26 | 24.66 |

In general, the resulting model exhibits a good fit for the experimental data. The range of the relative error is between 13% and 15% for the instaurations content and oxygen-oxirane content, respectively.

Table 3-11.Errors in the curve fitting

| | DB | OO |
|-------------------------|-----------|-----------|
| Absolute Error (AE) | 5.05 | 0.25 |
| Relative Error (RE) | 13.30 | 15.39 |
| Standard Deviation (SD) | 6.76 | 0.42 |

According to the results, the epoxidation reaction has a kinetic constant of $k_{0,2} = 5.96 \cdot 10^{-1}$ ($\text{L mol}^{-1} \text{ min}^{-1}$) at 333K, which is similar to that observed for the epoxidation of soybean oil [87]. However, the obtained value was higher than that observed in the epoxidation of methyl linoleate (i.e. $4.33 \cdot 10^{-2} \text{ L mol}^{-1} \text{ min}^{-1}$) [155]. This constant is one order of magnitude lower than the one reported in this work. However, in that model, oxirane cleavage reactions were not considered, so low values for this constant compensate the oxirane loss caused by ring-opening reactions. Also, the kinetic constant for the epoxidation reaction is higher than the peracetic acid formation $1.57 \cdot 10^{-2} (\text{L}^2 \text{ mol}^{-2} \text{ min}^{-1})$, verifying that peracid formation is the controlling step of the reaction [90].

As expected, due to the higher mobility and lower steric hindrance, the double bonds in the fatty esters are more reactive than those in TAGs. Consequently, the kinetic constant was larger than the other reported values. Similarly, the fatty acid composition of the feedstock has a significant effect on the rate constant of epoxidation. This is expected because conjugated double bonds in highly unsaturated fatty chains can be more prone to epoxidation. This has been previously observed and the reactivity of fatty acids in the epoxidation reaction follows the order: linolenic acid > linoleic acid > oleic acid as reported before [45].

Regarding the kinetic constants of oxirane degradation by acetic acid ($k_{0,3}$) and water ($k_{0,4}$), a ratio of $k_{0,3}/k_{0,4} = 48$ was obtained at 80°C. This result agrees with literature reports, which suggest that the attack by acetic acid proceeds at a higher rate. However, the concentration of acetic acid in the reaction medium is lower compared to the concentration of water. Moreover the degradation constants $k_{0,3}$ and $k_{0,4}$ increase rapidly with

temperature. Above 70°C these reactions are even competitive with the main epoxidation reaction [156].

At low temperatures, the rate of degradation is moderate, and the concentration of epoxide continuously increases. However, at high temperatures, the rate of epoxide degradation becomes higher than the rate of production, resulting in a decrease in the epoxide content. It's worth highlighting that the initial amount of acetic acid is lower than the amount required to degrade the epoxide, which confirms that water is also contributing to the degradation of the epoxide.

An example of a reasonably good fit of the obtained model is shown in Figure 3-20 which presents the experimental and regressed values for run *L11* performed at 50°C and molar ratios C=C:AA: HP (1:0.3:1.0). As observed, the predictions of double bonds and oxirane groups are well predicted. The complete set of experimental and fitted values is presented in annex D, where it is possible to confirm that the mathematical regression fits well all the experimental values.

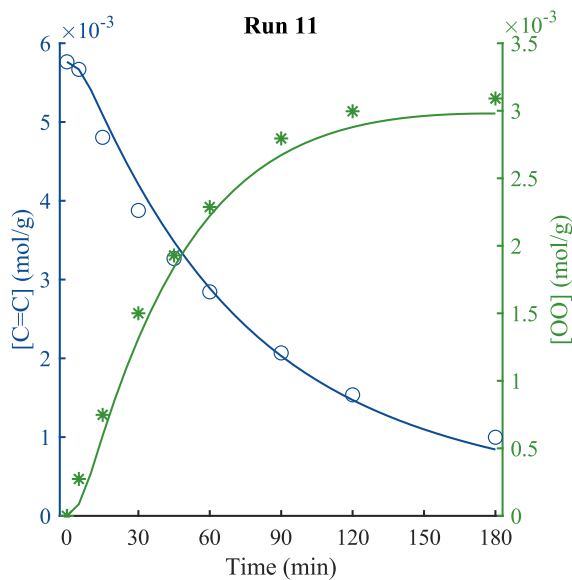


Figure 3-20. Fitted curves and experimental values for run L11.

Figure 3-21 presents the molar profiles (N) of each of the components over time. As seen, hydrogen peroxide (H_2O_2) and water (H_2O) are added dropwise into the reactor during the first 10 minutes. The molar profile of acetic acid in the oil phase (NAA_o) decayed after 120

minutes due to the oxirane degradation reaction (NDeg_1). In the case of peracetic acid, its concentration remains low as the reaction progresses. The aqueous phase is composed mostly of water, whose concentration remains steady over time.

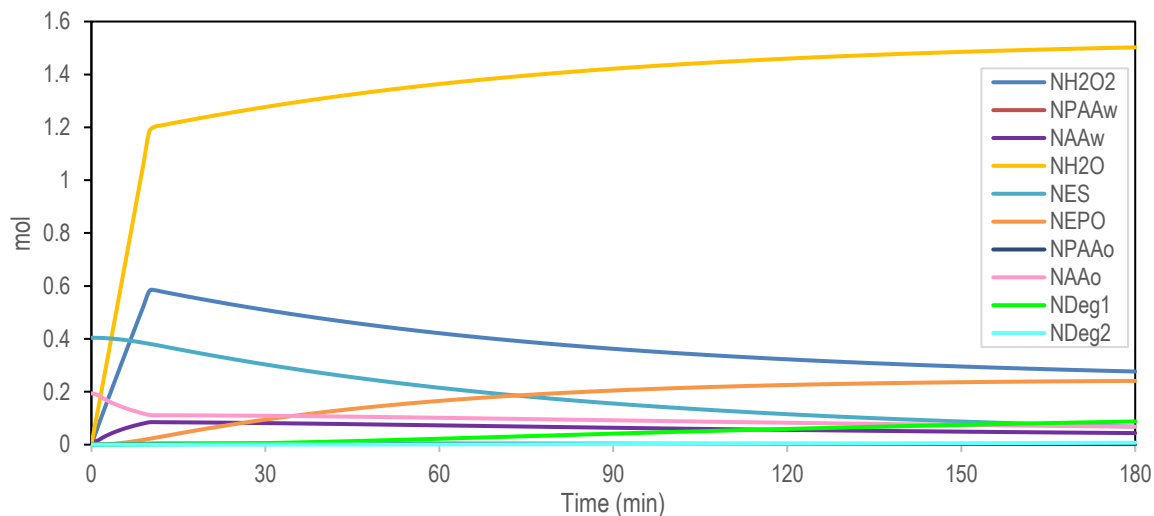


Figure 3-21. Molar profiles along the reaction time

Figure 3-22 shows the time evolution of the density and the volume of the two phases calculated over time. It can be verified that the volume and the density of each phase did not change significantly during the reaction.

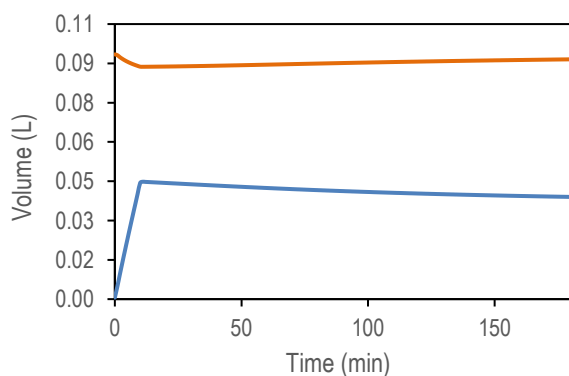


Figure 3-22. Volume along the reaction time

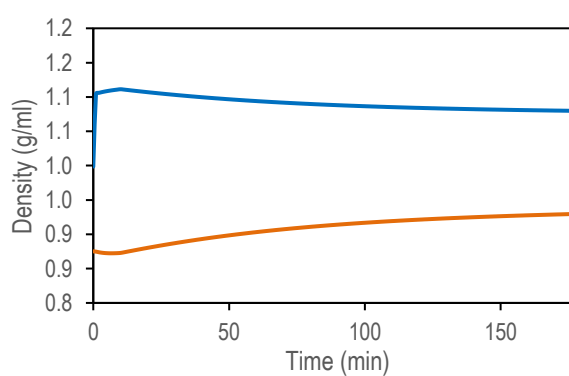
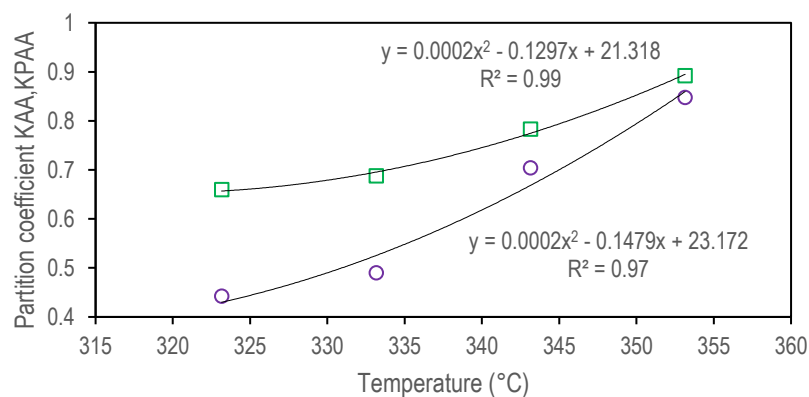


Figure 3-23. Density along the reaction time

Figure 3-24 presents the partition coefficients obtained from the regression parameters. In the epoxidation of isobutyl esters, the partition coefficient of acetic acid was found to be higher than that of peracetic acid. As the temperature increased, both partition coefficients increased in favor of a higher concentration of these compounds in the oleic phase. This

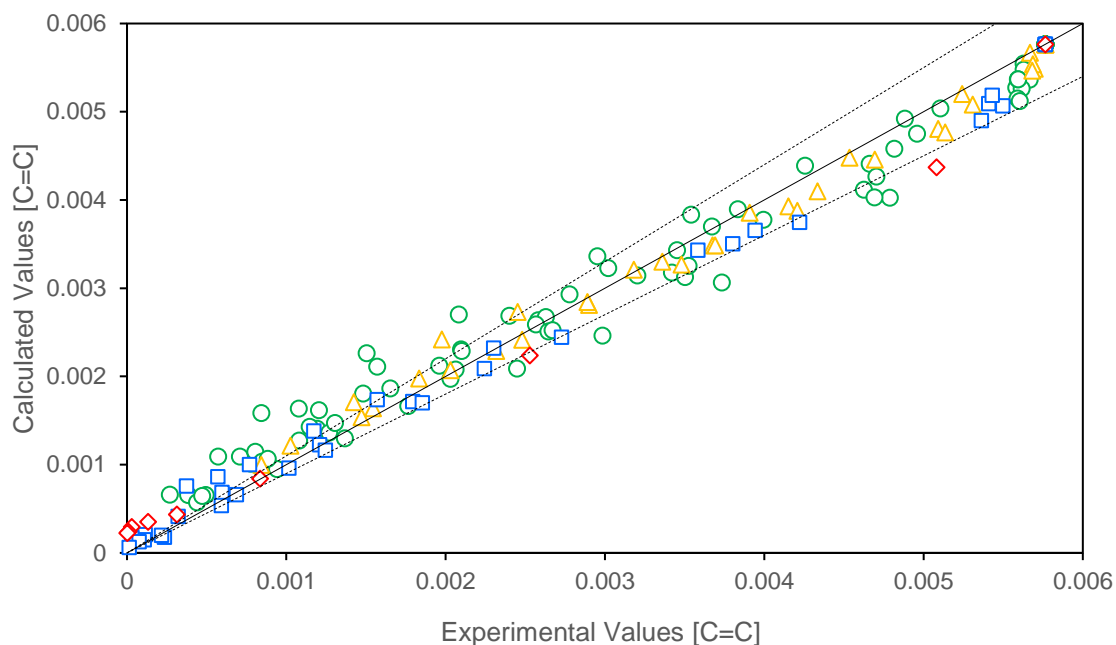
regression will employ to model the partition coefficient of acetic and peracetic acid in the optimization of the process conditions.



(□) Acetic acid partition coefficient (KAA) (○) Peracetic acid partition coefficient (KPAA)

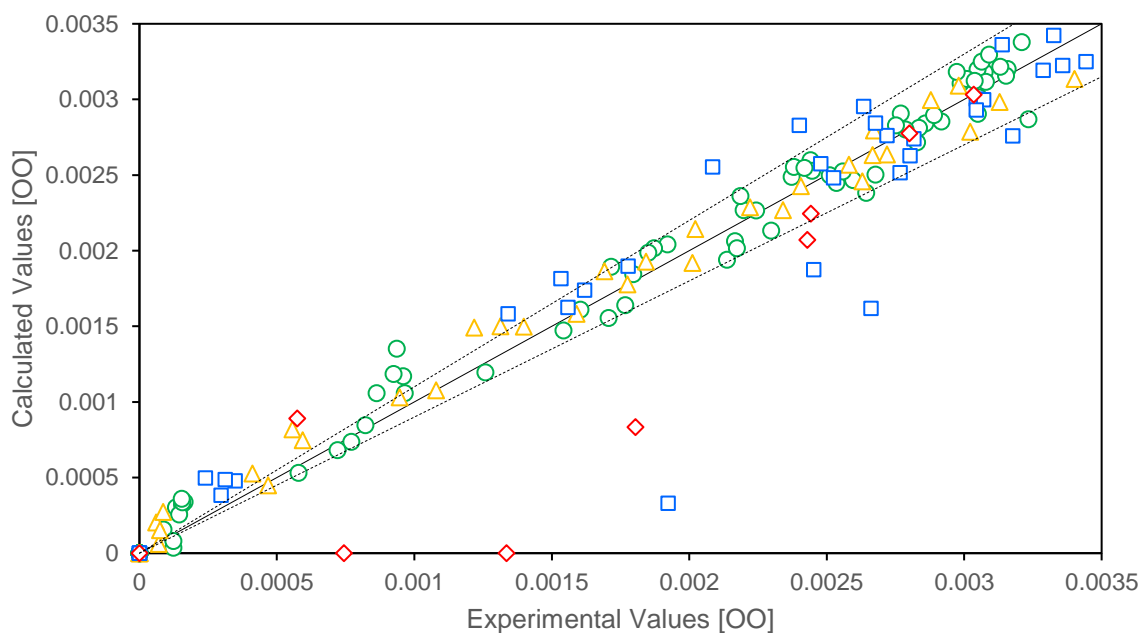
Figure 3-24. Regressed Partition coefficient

To visualize the good fit of the model, parity plots of all the experimental data and the predicted results used in the regression are presented in Figure 3-25 and Figure 3-26. In general, large differences were observed when operating at 70 and 80°C, as well as at long reaction times when the oxirane cleavage becomes more important and dilution effects caused by degradation products are significant. Regarding the iodine content, deviations from experimental values become noticeable at the end of the reaction. Experimental error plays a key role in the deviation of iodine value as at low concentrations, measurements are less accurate than at high concentrations.



(○) 60°C (△) 50°C (□) 70°C (◇) 80°C (---) ±10%

Figure 3-25. Parity plot of unsaturation content for all experimental runs



(○) 60°C (△) 50°C (□) 70°C (◇) 80°C (---) ±10%

Figure 3-26. Parity plot of oxirane oxygen content for all experimental runs

An important outcome of this work is that the regressed kinetic model can be used to estimate epoxidation rates for isobutyl esters of SODD and oleic acid [155]. It was stated that double bonds in oleic and linoleic acid exhibit similar epoxidation reactivity [155]. This model may have wider applications in the epoxidation of other raw materials, particularly during feasibility assessments and process design stages.

3.5 Optimization

The final step in this section is to identify the optimal reaction conditions for the epoxidation of fatty esters in a semi-batch reactor using the regressed kinetic parameters. The optimization objective is to maximize the oxirane oxygen of the epoxide and the global productivity of the process (Equation (3-43)).

$$Productivity = \frac{\text{mass of epoxide}}{\text{total mass}} * 100 \quad (3-42)$$

As described in the previous section, besides the epoxide formation other undesirable reactions occur in the reaction medium. Hence, to achieve high epoxide yields, the production of these degradation products must be minimized. With this goal in mind, the objective function was constructed, as shown in Equation (3-43).

$$Objective\ function = Conversion * Selectivity \quad (3-43)$$

The parameters to be optimized are temperature, molar ratio of reagents, and the amount of catalyst. Table 3-12 displays the optimization parameters of the search space during the optimization process. For the assessment, 70g of isobutyl ester was considered. It is important to note that a high oxirane content can be achieved not only by carrying out the epoxidation at moderate temperatures but also by limiting the reaction time at higher temperatures. The first route accounts for less use of catalyst than the second.

Table 3-12. Optimization variables range

| Variable | Lower limit | Upper limit |
|--|-------------|-------------|
| Temperature (°C) | 40 | 80 |
| Molar ratio H ₂ O ₂ :C=C | 1 | 2.5 |

| | | |
|--------------------|------|-----|
| Catalyst %(w/w) | 0.50 | 5 |
| Molar ratio AA:C=C | 0.2 | 1 |
| Time (min) | 5 | 540 |

The optimal conditions for the epoxidation of isobutyl esters, determined using the regressed model and a semi-batch reactor, are presented in Table 3-13. Under these conditions, the highest yield of oxirane was (80.3%) using sulfuric acid as a catalyst.

Table 3-13. Optimization results

| Variable | Value |
|--|-------|
| Temperature (°C) | 60.5 |
| Molar ratio C=C: H ₂ O ₂ | 3.0 |
| Catalyst %(w/w) | 1.57 |
| Molar ratio C=C: AA | 0.21 |
| Time (min) | 355 |
| OO(%) | 6.58 |
| Yield (%) | 80.3 |
| Conversion (%) | 95.4 |
| Selectivity (%) | 84.2 |

As a result of the optimization, mild conditions for temperature and catalyst loading were obtained. The molar profile of each component is displayed in Figure 3-28. These operation conditions favor the production of epoxide while minimizing the formation rates of degradation products. Additionally, controlled rates of oxirane cleavage are achieved due to the low concentration of sulfuric acid and acetic acid in the system. The resulting oxirane content is 6.6%, which corresponds to 78% of the maximum theoretical value of oxirane. This outcome highlights the importance of seeking new catalysts with high activity and selectivity for the synthesis of epoxides, such as ion exchange resins.

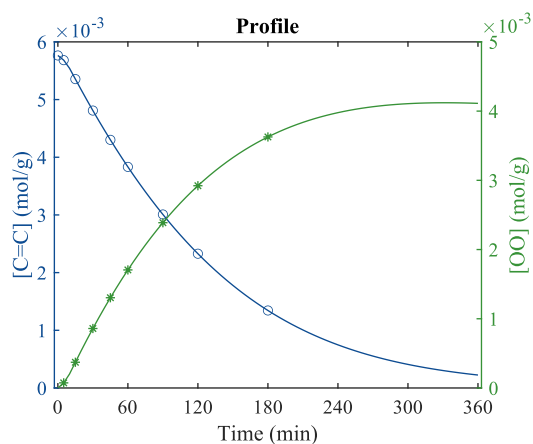


Figure 3-27. Concentration of oxirane and double bonds for the optimum conditions

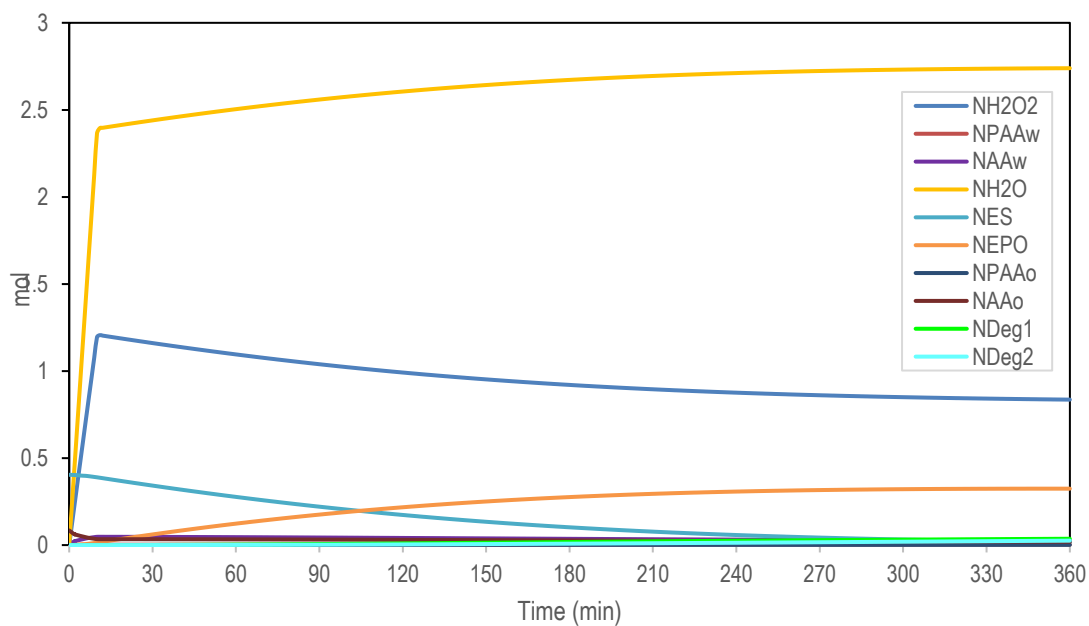


Figure 3-28. Molar profiles along the reaction time for the optimum conditions

3.6 Plasticizers production at bench scale and characterization

Epoxides of isobutanol, namely: epoxide of isobutyl oleate (EIO), epoxide of isobutyl linoleate (EIL), epoxidized isobutyl soyate distillate (EID), and epoxide of isobutyl soyate

(EIS), were produced at bench scale by following the methodology described in the previous section. However, the main goal of this stage was to produce enough amount of epoxides for further evaluation as plasticizers, and thus it was necessary to maximize oxirane content, reduce ring-opening decomposition, and avoid product darkening. For this reason, larger bench-scale batches were carried out at the conditions that optimized oxirane productivity but with a different catalyst. In this case, an ion exchange resin (Amberlyst IRC 120 H) was used as a catalyst with the same acid equivalents of H_2SO_4 determined under the optimal conditions. Considering the ion exchange capacity of the resin, and the molecular weight of H_2SO_4 , it was found that the equivalent loading of the resin to the acid was 5.48 ± 0.07 g resin/g H_2SO_4 . As the heterogeneous catalyst is less active and might present lower mass transfer rates, the reaction time was set at 6 hours. Once completed, the heterogeneous catalyst was removed from the reaction mixture by filtration, and there was no need for neither further neutralization or bleaching.

The main physicochemical characteristics of the obtained epoxides at the bench scale are presented in Table 3-14, and the appearance of the resulting products is shown in Figure 3-29.

Table 3-14. Characterization of isobutyl epoxides

| Property | EIO | EIL | EID | EIS |
|-------------------------------------|-----------------|-----------------|-----------------|-----------------|
| Acid value (mg KOH/g) | 0.8 ± 0.2 | 1.1 ± 0.3 | 1.0 ± 0.2 | 2.0 ± 0.2 |
| Iodine value (g I_2 /100g) | 9.3 ± 0.7 | 12.5 ± 0.9 | 8.9 ± 0.4 | 12.7 ± 0.1 |
| Oxirane Oxygen (%) | 4.47 ± 0.1 | 6.31 ± 0.1 | 4.1 ± 0.2 | 4.2 ± 0.1 |
| Moisture (%) | 0.12 | 0.15 | 0.16 | 0.10 |
| MW calculated | 359.3 ± 0.7 | 371.4 ± 0.9 | 429.7 ± 0.4 | 476.7 ± 0.1 |
| Density (20°C) (kg/m^3) | 929.7 | 955.5 | 920.2 | 936.0 |
| Density (40°C) (kg/m^3) | 911.7 | 937.5 | 902.2 | 920.0 |
| Kinematic Viscosity (40°C) (cSt) | 14.8 ± 0.1 | 17.1 ± 0.1 | 11.6 ± 0.1 | 20.9 ± 0.6 |
| Dynamic Viscosity (40°C) (cP) | 13.5 ± 0.1 | 16.0 ± 0.1 | 10.5 ± 0.1 | 19.2 ± 0.6 |
| Color | Yellow | Yellow | Yellow | Orange |



Figure 3-29. Produced epoxidized isobutyl esters at the bench scale.

(a) Isobutyl Oleate (EIO) (b) Epoxidized Isobutyl Linoleate (EIL) (c) Epoxidized isobutyl soyate distillate (EID) (d) Epoxidized Isobutyl Soyate (EIS)

The molar weight of the isobutyl epoxides in Table 3-14 was calculated based on the molar weight of the esters and their iodine value. Isobutyl epoxides EIO, EIL, EID, and EIS meet most of the parameters of epoxidized esters as listed in Table 1-10. However, it is necessary to reduce their final iodine value (9-13 cg I₂/g). For further epoxidation, it would be necessary to extend the reaction time to decrease the iodine value below the recommended level for oleochemical plasticizers. In the case of epoxidized isobutyl soyate, a bleaching treatment would be necessary to improve the color of the final product. If this is not possible, the application of these epoxides would be limited to products that do not require clear or translucent specifications.

The dynamic viscosity of the final product follows the order EIS> EIL>EIO>EID with viscosity values ranging from 10.5 to 19.2 cP. This is about three times higher than their corresponding isobutyl ester. As expected, the introduction of oxygen in the double bond increases the viscosity of the product due to the more polar interaction of the oxirane rings. The obtained viscosity of the epoxidized isobutyl ester is in the range of other oleochemical epoxides and even of some phthalates. Reference plasticizers such as epoxidized soybean and DOP have dynamic viscosities of 13 cP at 40°C and 26 cP at 40°C, respectively [79], [157].

- Thermal properties of epoxides

To study the thermal properties of the epoxides (EIO, EIL, EID, and EIS), the samples were analyzed using the same thermal cycles (crystallization and melting) that were employed to evaluate the thermal properties of esters.

The crystallization and melting cycles of isobutyl epoxides obtained at the bench scale are shown in Figure 3-30 and Figure 3-31. Furthermore, the thermal degradation of these epoxides is presented in Figure 3-32.

As observed, isobutyl epoxides exhibited several peaks in the DSC thermogram, which explains why they crystallize and melt over a wide range of temperatures. The results were analyzed based on the main thermal peaks. In general, isobutyl epoxides exhibited good thermal properties for plasticizing purposes. All these epoxides have low crystallization temperatures in the range of -22 to -35°C. Likewise, they exhibited low melting points between -14 and -17°C. This indicates that they can also be used in different industrial applications, such as lubricants, surfactants, or even as additives for fuels where good fluidization at low temperatures is required [158].

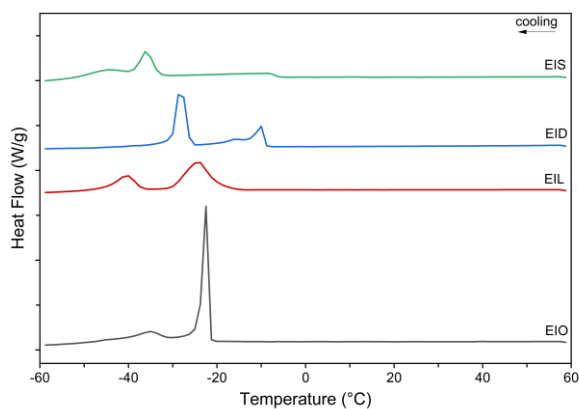


Figure 3-30. Crystallization DSC curves of isobutyl epoxides

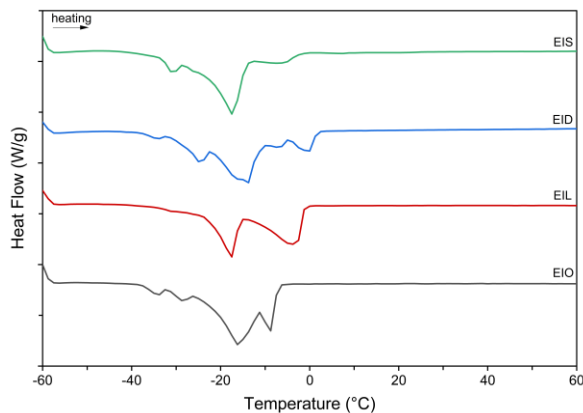
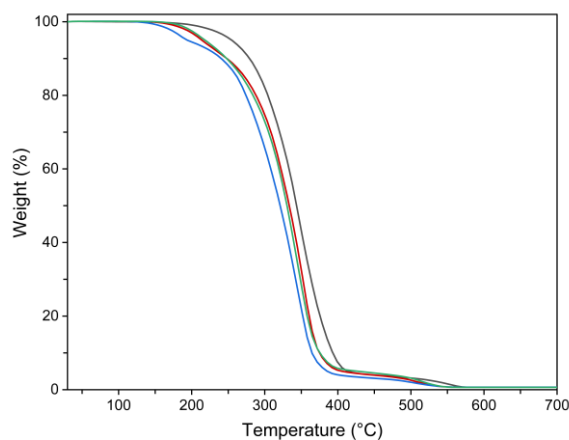


Figure 3-31. Melting DSC curves of isobutyl epoxides



(— IBO) (— IBL) (— ISD) (— ISO)
Figure 3-32. Thermal degradation of isobutyl epoxides

In particular, the thermal properties of the isobutyl esters and epoxides are enhanced after the functionalization of the molecule by esterification and epoxidation. Similar results have been found in the study of the cold flow properties of epoxidized castor oil [159]. The thermal stability of epoxides is slightly higher than the corresponding ester and fatty acids, which is attributed to the incorporation of oxygen instead a double bond that is more easily oxidized.

- FTIR of bench-scale epoxides

The main groups of the assessed epoxide molecules were identified through FTIR spectra. The peak at 819 cm^{-1} is associated with oxirane oxygen vibration. Additionally, the peaks at 1724 cm^{-1} and 1285 are related to the C=O and C-O vibrations of ester groups respectively [160]. Figure 3-33 presents the characteristic absorbance of these compounds.

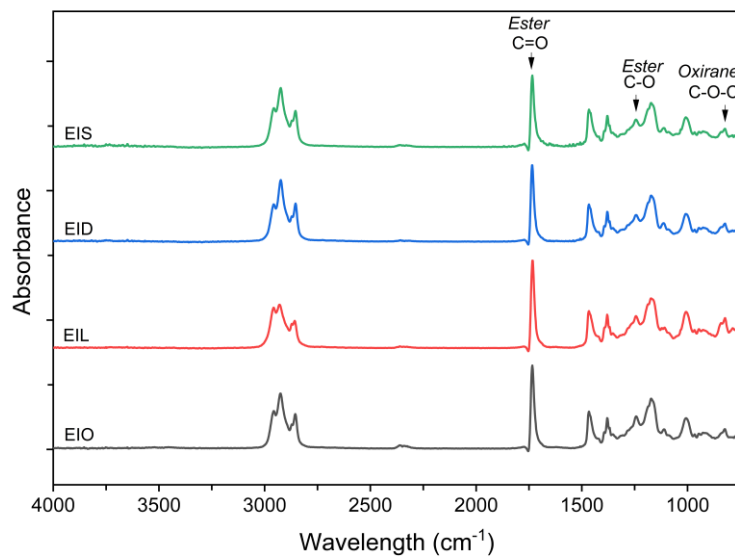


Figure 3-33. FTIR spectra of isobutyl epoxides